

We thank editor's comments. The editor's comments are listed in *italics*, and our responses in black with revised texts in **bold black**.

Dear Authors,

The reviewers' comments have been well taken into account. However, the question of Reviewer #2 about the missing version number of the retrieval algorithm, brings me to the question whether the data product has a version number? And whether the data product is available to users? Could you specify that at the end of the paper?

The version number of PROFOZ is 0.9.3. This data product is available to users at Aura Validation Data Center (AVDC).

We have added a data availability section at the end of this paper as:

“OMI PROFOZ (version 0.9.3) used in this study is available to users at Aura Validation Data Center (AVDC) (<https://avdc.gsfc.nasa.gov/index.php?site=1389025893&id=74>).”

In addition, we have updated our data link at first paragraph of the Introduction section as:

“The ozone profile product titled PROFOZ is publicly available at the Aura Validation Data Center (AVDC) (<https://avdc.gsfc.nasa.gov/index.php?site=1389025893&id=74>).”

Textual corrections:

- *Caption Figure 8: Scattering plot > Scatter plot*

Done.

- *Caption of Figures 11 and 12: "Fig. 9but " has a missing space*

Done.

1 **Validation of 10-year SAO OMI Ozone Profile (PROFOZ)**

2 **Product Using Ozonesonde Observations**

3

4 Guanyu Huang^{1,*}, Xiong Liu¹, Kelly Chance¹, Kai Yang², Pawan K. Bhartia³, Zhaonan Cai¹,
5 Marc Allaart⁴, Gérard Ancellet⁵, Bertrand Calpini⁶, Gerrie J. R. Coetzee⁷, Emilio Cuevas-
6 Agulló⁸, Manuel Cupeiro⁹, Hugo De Backer¹⁰, Manvendra K. Dubey¹¹, Henry E. Fuelberg¹²,
7 Masatomo Fujiwara¹³, Sophie Godin-Beekmann⁵, Tristan J. Hall¹², Bryan Johnson¹⁴, Everette
8 Joseph¹⁵, Rigel Kivi¹⁶, Bogumil Kois¹⁷, Ninong Komala¹⁸, Gert König-Langlo¹⁹, Giovanni
9 Laneve²⁰, Thierry Leblanc²², Marion Marchand, Kenneth R. Minschwaner²³, Gary Morris²⁴,
10 Michael J. Newchurch²⁵, Shin-Ya Ogino²⁶, Nozomu Ohkawara²⁷, Ankie J. M. Pitters⁴, Françoise
11 Posny²⁸, Richard Querel²⁹, Rinus Scheele⁴, Frank J. Schmidlin³, Russell C. Schnell¹⁴, Otto
12 Schrems¹⁹, Henry Selkirk³⁰, Masato Shiotani³¹, Pavla Skrivánková³², René Stübi⁶, Ghassan
13 Taha³⁰, David W. Tarasick³³, Anne M. Thompson³, Valérie Thouret³⁴, Matt Tully³⁵, Roeland
14 van Malderen¹⁰, , Holger Vömel³⁶, Peter von der Gathen³⁷, Jacquelyn C. Witte³⁸, Margarita
15 Yela³⁹

- 16 1. Harvard-Smithsonian Center for Astrophysics, Cambridge, MA, USA
17 2. Department of Atmospheric and Oceanic Science, University of Maryland, College Park,
18 Maryland, USA
19 3. NASA Goddard Space Flight Center, Greenbelt, Maryland, USA
20 4. Royal Netherlands Meteorological Institute (KNMI), De Bilt, the Netherlands
21 5. LATMOS-ISPL, Université Paris 6 Pierre-et-Marie-Curie, Paris, France
22 6. MeteoSwiss Aerological Station, Federal Office of Meteorology and Climatology
23 MeteoSwiss, Payerne, Switzerland
24 7. South African Weather Service, Pretoria, South Africa
25 8. Izana Atmospheric Research Center, Meteorological State Agency of Spain, Santa Cruz de
26 Tenerife, Spain
27 9. National Meteorological Service, Ushuaia, Tierra del Fuego, Argentina
28 10. Royal Meteorological Institute of Belgium, Brussel, Belgium
29 11. Los Alamos National Laboratory, Los Alamos, NM, USA

- 30 12. Earth, Ocean and Atmospheric Sciences, Florida State University, Tallahassee, FL, USA
31 13. Faculty of Environmental Earth Science, Hokkaido University, Sapporo, Japan
32 14. NOAA/ESRL Global Monitoring Division, Boulder, CO, USA
33 15. Atmospheric Sciences Research Center, SUNY University at Albany, Albany, NY, USA
34 16. Finnish Meteorological Institute, Helsinki, Finland
35 17. The Institute of Meteorology and Water Management, National Research Institute, Warsaw,
36 Poland
37 18. Indonesian Institute of Aeronautics and Space (LAPAN), Bandung, Indonesia
38 19. Alfred Wegener Institute for Polar and Marine Research, Bremerhaven, Germany
39 20. Earth Observation Satellite Images Applications Lab (EOSIAL), Università di Roma 'La
40 Sapienza', Rome, Italy
41 21. Danish Meteorological Institute, Copenhagen, Denmark
42 22. Jet Propulsion Laboratory, California Institute of Technology, Pasadena, CA, USA
43 23. Department of Physics, New Mexico Institute of Mining and Technology, Socorro, NM,
44 USA
45 24. St. Edward's University, Austin, TX, USA
46 25. Department of Atmospheric Science, University of Alabama in Huntsville, Huntsville, AL,
47 USA
48 26. Department of Coupled Ocean-Atmosphere-Land Processes Research, Japan Agency for
49 Marine-Earth Science and Technology, Yokosuka, Japan
50 27. Global Environment and Marine Department, Japan Meteorological Agency, Tokyo, Japan
51 28. Université de la Réunion, Saint Denis, France
52 29. National Institute of Water and Atmospheric Research, Lauder, Central Otago, New Zealand
53 30. Universities Space Research Association, Greenbelt, MD, USA
54 31. Research Institute for Sustainable Humanosphere, Kyoto University, Kyoto, Japan
55 32. Upper Air and Surface Observation Department, Czech Hydrometeorological Institute,
56 Praha, Czech Republic
57 33. Air Quality Research Division, Environment & Climate Change Canada, Downsview, ON,
58 Canada.
59 34. Laboratoire d'Aerologie, Université de Toulouse, Toulouse, France

- 60 35. Observations & Infrastructure Division, Bureau of Meteorology, Melbourne, Victoria,
61 Australia
- 62 36. Earth Observing Laboratory, National Center for Atmospheric Research, Boulder, CO, USA
- 63 37. Alfred Wegener Institute, Potsdam, Germany
- 64 38. Science Systems and Applications Inc. Greenbelt, MD, USA
- 65 39. Atmospheric Research and Instrumentation Branch, National Institute for Aerospace
66 Technology (INTA), Madrid, Spain
- 67 *Correspondence to: Guanyu Huang (guanyu.huang@cfa.harvard.edu)

68 **Abstract**

69 We validate the Ozone Monitoring Instrument (OMI) ozone-profile (PROFOZ) product from
70 October 2004 through December 2014 retrieved by the Smithsonian Astrophysical Observatory
71 (SAO) algorithm against ozonesonde observations. We also evaluate the effects of OMI Row
72 anomaly (RA) on the retrieval by dividing the data set into before and after the occurrence of
73 serious OMI RA, i.e., pre-RA (2004-2008) and post-RA (2009-2014). The retrieval shows good
74 agreement with ozonesondes in the tropics and mid-latitudes and for pressure < ~50 hPa in the
75 high latitudes. It demonstrates clear improvement over the a priori down to the lower troposphere
76 in the tropics and down to an average of ~550 (300) hPa at middle (high latitudes). In the tropics
77 and mid-latitudes, the profile mean biases (MBs) are less than 6%, and the standard deviations
78 (SDs) range from 5-10% for pressure < ~50 hPa to less than 18% (27%) in the tropics (mid-
79 latitudes) for pressure > ~50 hPa after applying OMI averaging kernels to ozonesonde data. The
80 MBs of the stratospheric ozone column (SOC, the ozone column from the tropopause pressure to
81 the ozonesonde burst pressure) are within 2% with SDs of < 5% and the MBs of the tropospheric
82 ozone column (TOC) are within 6% with SDs of 15%. In the high latitudes, the profile MBs are
83 within 10% with SDs of 5-15% for pressure < ~50 hPa, but increase to 30% with SDs as great as
84 40% for pressure > ~50 hPa. The SOC MBs increase up to 3% with SDs as great as 6% and the
85 TOC SDs increase up to 30%. The comparison generally degrades at larger solar-zenith angles
86 (SZA) due to weaker signals and additional sources of error, leading to worse performance at
87 high latitudes and during the mid-latitude winter. Agreement also degrades with increasing
88 cloudiness for pressure > ~100 hPa and varies with cross-track position, especially with large
89 MBs and SDs at extreme off-nadir positions. In the tropics and mid-latitudes, the post-RA
90 comparison is considerably worse with larger SDs reaching 2% in the stratosphere and 8% in the
91 troposphere and up to 6% in TOC. There are systematic differences that vary with latitude
92 compared to the pre-RA comparison. The retrieval comparison demonstrates good long-term
93 stability during the pre-RA period, but exhibits a statistically significant trend of 0.14-0.7%/year
94 for pressure < ~ 80 hPa, 0.7 DU/year in SOC and -0.33 DU/year in TOC during the post-RA
95 period. The spatiotemporal variation of retrieval performance suggests the need to improve
96 OMI's radiometric calibration especially during the post-RA period to maintain the long-term
97 stability and reduce the latitude/season/SZA and cross-track dependence of retrieval quality.

98 **1 Introduction**

99 The Dutch-Finnish built Ozone Monitoring Instrument (OMI) on board the NASA Aura satellite
100 has been making useful measurements of trace gases including ozone and aerosols since October
101 2004. There are various retrieval algorithms to retrieve ozone profile and/or total ozone from
102 OMI data (Bak et al., 2015), including two independent operational total ozone algorithms
103 (Bhartia and Wellemeyer, 2002; Veefkind et al., 2006) and two ozone profile algorithms. Of the
104 two ozone profile algorithms, one is the operational algorithm (OMO3PR) developed at KNMI
105 (van Oss et al., 2001), and the other one is a research algorithm developed at Smithsonian
106 Astrophysical Observatory (SAO) by (Liu et al., 2010b). Both algorithms retrieve ozone profile
107 from the spectral region 270-330 nm using the optimal estimation method, but they differ
108 significantly in implementation details including radiometric calibration, radiative transfer model
109 simulation, a priori constraint, retrieval grids, and additional retrieval parameters. The SAO
110 ozone profile retrieval algorithm was initially developed for Global Ozone Monitoring
111 Experiment (GOME) data and was adapted to OMI data (Liu et al., 2010b). Total ozone column
112 (OC), Stratospheric Ozone Column (SOC) and Tropospheric Ozone Column (TOC) can be
113 directly derived from the retrieved ozone profile with retrieval errors in the range of a few
114 Dobson Units (DU) (Liu et al., 2006b; Liu et al., 2010a). This algorithm has been put into
115 production in the OMI Science Investigator-led Processing System (SIPS), processing the entire
116 OMI data record with approximately one-month delay. The ozone profile product titled
117 PROFOZ is publicly available at the Aura Validation Data Center (AVDC)
118 (<https://avdc.gsfc.nasa.gov/index.php?site=1389025893&id=74>
119 <http://avdc.gsfc.nasa.gov/index.php?site=2045907950>). This long-term ozone profile product, with high spatial resolution and
120 daily global coverage, constitutes a useful dataset to study the spatial and temporal distribution
121 of ozone.

122 To effectively use the retrieval dataset, it is necessary to evaluate and understand its retrieval
123 quality and long-term performance. Although validation of the ozone profile product (mostly
124 earlier versions) has been partially performed against aircraft, ozonesonde, and Microwave Limb
125 Sounder (MLS) data, these evaluations are limited to certain time periods and/or spatial region
126 and/or to only portion of the product (e.g., total ozone columns (OC) or TOC only) (Bak et al.,
127 2013a; Hayashida et al., 2015; Lal et al., 2013; Liu et al., 2010a; Liu et al., 2010b; Pittman et al.,

128 2009; Sellitto et al., 2011; Wang et al., 2011; Yang et al., 2007; Ziemke et al., 2014).
129 Additionally, the quality of ozone profile retrievals is very sensitive to the signal to noise ratio
130 (SNR) of the radiance measurements as well as their radiometric calibration, which may degrade
131 over time as shown in GOME and GOME-2 retrievals (Cai et al., 2012; Liu et al., 2007).
132 Although OMI's optical degradation is remarkably small to within 1-2% over the years, the SNR
133 and the number of good spectral pixels (not flagged as bad/hot pixels) have been gradually
134 decreasing over the years due to the expected CCD degradation (Claas, 2014). Furthermore, the
135 occurrence of RA, which affects level 1b data at all wavelengths for particular viewing directions
136 or cross-track positions and likely due to blocking objects in the optical path, started in June
137 2007 affecting a few positions. This effect abruptly worsened in January 2009 affecting ~1/3 of
138 the cross-track positions (Kroon et al., 2011). The impacts of RA not only evolve with time but
139 also vary over the duration of an orbit. Analysis indicates that radiances in the UV1 channels
140 (shorter than ~310 nm) used in our retrievals might have been affected at all positions (Personal
141 communication with S. Marchenko) and are not adequately flagged for RA. Therefore, we need
142 to evaluate the impacts of instrument degradation and especially row anomaly on the temporal
143 performance of our ozone profile product. Currently, we are planning an update of the ozone
144 profile algorithm to maintain the long-term consistency of the product. The update will include
145 empirical correction of systematic errors caused by the instrument degradation and row anomaly
146 as a function of time. Such correction also requires us to evaluate the long-term retrieval quality
147 of our product.

148 To understand retrieval quality and the resulting spatial and temporal performance of our OMI
149 product, we evaluate our data from October 2004 through December 2014 against available
150 ozonesonde and MLS observations, respectively, in two papers. This paper evaluates our ozone
151 product including both ozone profiles and stratospheric and tropospheric ozone columns using
152 ozonesonde observations with a focus on retrieval quality in the troposphere. More than 27,000
153 ozonesonde profiles from both regular ozonesonde stations and field campaigns are used in this
154 study to provide a comprehensive and global assessment of the long-term quality of our OMI
155 ozone product. This paper is followed by the validation against collocated MLS data with a focus
156 on the retrieval quality in the stratosphere (Huang et al., 2017), also submitted to this special
157 issue).

158 This paper is organized as follows: Section 2 describes OMI retrievals and ozonesonde data. The
159 validation methodology is introduced in Section 3. Section 4 presents results, analysis and
160 discussions regarding the OMI and ozonesonde comparisons. Section 5 summarizes and
161 concludes this study.

162 **2 OMI and Ozonesonde Datasets**

163 **2.1 OMI and OMI Ozone Profile Retrievals**

164 OMI is a Dutch-Finnish built nadir-viewing pushbroom UV/visible instrument aboard the NASA
165 Earth Observing System (EOS) Aura satellite that was launched into a sun-synchronous orbit in
166 July 2004. It measures backscattered radiances in three channels covering the 270-500 nm
167 wavelength range (UV1: 270-310 nm, UV2: 310-365 nm, visible: 350-500 nm) at spectral
168 resolutions of 0.42-0.63 nm (Levelt et al., 2006). Measurements across the track are binned to
169 60 positions for UV2 and visible channels, 30 positions for the UV1 channels due to the weaker
170 signals. This results in daily global coverage with a nadir spatial resolution of 13 km × 24 km
171 (along × across track) for UV2 and visible channels, and 13 km × 48 km for the UV1 channel.

172 The SAO OMI ozone profile algorithm was adapted from the GOME ozone profile algorithm
173 (Liu et al., 2005) to OMI and was initially described in detail in Liu et al. (2010b). Profiles of
174 partial ozone columns are retrieved at 24 layers, ~2.5 km for each layer, from the surface to ~60
175 km using OMI radiance spectra in the spectral region 270-330 nm with the optimal estimation
176 technique. In addition to the OC, SOC and TOC can be directly derived from the retrieved ozone
177 profile with the use of tropopause (defined based on the lapse rate) from the daily National
178 Center for Environmental Protection (NCEP) reanalysis data. The retrievals are constrained with
179 month- and latitude-dependent climatological a priori profiles derived from 15-year ozonesonde
180 and SAGE/MLS data (McPeters et al., 2007) with considerations of OMI random-noise errors.
181 OMI radiances are pre-calibrated based on two days of average radiance differences in the
182 tropics between OMI observations and simulations with zonal mean MLS data for pressure less
183 than 215 hPa and climatological ozone profile for pressure greater than 215 hPa. This “soft
184 calibration” varies with wavelength and cross-track positions but does not depend on space and
185 time.

186 The current algorithm of our SAO OMI ozone product that is used in this paper was briefly
187 described in Kim et al. (2013). The radiative transfer calculations have been improved through
188 the convolution of simulated radiance spectra at high resolutions rather than effective cross
189 sections, which is done by interpolation from calculation at selected wavelengths assisted by
190 weighting function. In addition, four spatial pixels along the track are coadded to speed up
191 production processes at a nadir spatial resolution of 52 km × 48 km. Meanwhile, minimum
192 measurement errors of 0.4% and 0.2% are imposed in the spectral ranges 270-300 nm and 300-
193 330 nm, respectively, to stabilize the retrievals. The use of floor errors typically reduces the
194 Degree of Freedom for Signals (DFS) and increases retrieval errors. Compared to the initial
195 retrievals, the average total, stratospheric, and tropospheric DFS decrease by 0.49, 0.27, and
196 0.22, respectively, and the mean retrieval errors in OC, SOC, and TOC increase by 0.6, 0.5, and
197 1.2 DU, respectively. The corresponding changes to the retrievals are generally within retrieval
198 uncertainties except for a systematic increase in tropospheric ozone at SZA larger than ~75°,
199 where the TOC increases to ~12 DU. Validation against ozonesonde data indicates that this TOC
200 increase at large SZA makes the retrieval worse. Therefore retrieved tropospheric ozone at such
201 large SZA should not be used, but the retrieved total ozone still shows good quality (Bak et al.,
202 2015).

203 For current products, retrievals contain ~5.5-7.4 DFS, with 4.6-7.3 in the stratosphere and 0-1.2
204 in the troposphere. Vertical resolution varies generally from 7–11 km in the stratosphere to 10–
205 14 km in the troposphere, when there is adequate retrieval sensitivity to the tropospheric ozone.
206 Retrieval random-noise errors (i.e., precisions) typically range from 0.6–2.5 % in the middle
207 stratosphere to approximately 12% in the lower stratosphere and troposphere. The solution
208 errors, dominated by smoothing errors, vary generally from 1-7% in the middle stratosphere to 7-
209 38% in the troposphere. The solution errors in the integrated OC, SOC, and TOC are typically in
210 the few DU range. Errors caused by the forward model and forward model parameter
211 assumptions are generally much smaller than the smoothing error (Liu et al., 2005). The main
212 sources of these errors include systematic errors in temperature and cloud-top pressure.
213 Systematic measurement errors are the most difficult to estimate, mostly due to lack of full
214 understanding of the OMI instrument calibration.

215 Certain cross track positions in OMI data have been affected by RA since June 2007 (Kroon et
216 al., 2011). Loose thermal insulating material in front of the instrument's entrance slit is believed
217 to block and scatter light, causing measurement error. The anomaly affects radiance
218 measurements at all wavelengths for specific cross-track viewing directions that are imaged to
219 CCD rows. Initially, the anomaly only affected a few rows. But since January 2009, the anomaly
220 has spread to other rows and shifted with time. The RA also shows slight differences among
221 different spectral channels, and varies during the duration of an orbit. Pixels affected by the RA
222 are flagged in the level 1b data. The science team suggested that they are not be used in research.
223 For data before 2009, the RA flagging is not applied in the processing. Pixels seriously affected
224 by RA will typically show enhanced fitting residuals. The algorithm was updated to use RA
225 flagging in the UV1 channel and was used to process the data starting from 2009. If a pixel is
226 flagged as a row anomaly then it is subsequently not retrieved to speed up the processing except
227 that the cross-track position 24 is still retrieved due to reasonably good fitting. It should be noted
228 that the retrieval quality of those non-flagged pixels may still be affected by the RA, because of
229 the different RA flagging in the UV1 and UV2, the lack of RA flagging before 2009 and
230 inadequacy of the RA flagging.

231 To screen out OMI profiles for validation, we only use OMI ozone profiles meeting the
232 following criteria based on three filtering parameters: 1) nearly clear-sky scenes with effective
233 cloud fraction less than 0.3; 2) cross track positions between 4 and 27, due to the relatively worse
234 quality and much larger footprint size of the off-nadir pixels beyond this range; 3) SZA should
235 be less than 75° due to very limited retrieval sensitivity to tropospheric ozone and the
236 aforementioned positive biases. The selection and justification of these criteria will be discussed
237 in Sects. 2.1.2-4.1.4, in which we will use all OMI pixels of each filtering parameter when
238 evaluating retrieval quality as a function of that specific parameter. The fitting quality of each
239 retrieval is shown in the fitting RMS (root mean square of the fitting residuals relative to the
240 assumed measurement errors). The mean fitting RMS including both UV1 and UV2 channels has
241 been increasing with time as shown in Figure 1. This is primarily due to the increase of fitting
242 residuals in UV1 caused by the instrument degradation and RA since the fitting residuals of UV2
243 only slightly increase with time. As aforementioned, the retrieval information of stratospheric
244 and tropospheric ozone mainly comes from UV1 and UV2, respectively. Consequently, retrievals

245 in the troposphere, the focus of this paper, are less impacted by the increasing fitting RMS.
246 However, to apply consistent filtering in validation against both ozonesonde in this study and
247 MLS data in the companion paper (Huang et al., 2017), we set the RMS threshold based on the
248 overall fitting RMS and select retrievals with fitting RMS smaller than the sum of monthly mean
249 RMS and its 2σ (i.e., Standard Deviations (SDs) of fitting RMS).

250 **2.2 Ozonesondes**

251 The balloon-borne ozonesonde is a well-established technique to observe the ozone profile from
252 the surface to ~35 km with vertical resolution of ~100-150 m and approximately 3-5% precision
253 and 5-10% accuracy (Deshler et al., 2008; Johnson, 2002; Komhyr, 1986; Komhyr et al., 1995;
254 Smit et al., 2007). Ozonesonde data have been widely used in the studies of stratospheric ozone,
255 climate change, tropospheric ozone and air quality, as well as the validation of satellite
256 observations (Huang et al., 2015; Kivi et al., 2007; Thompson et al., 2015; Wang et al., 2011).
257 However, the accuracy of ozonesonde observations depends on data processing technique, sensor
258 solution, and instrument type and other factors. Consequently, station-to-station biases may
259 occur in ozonesonde measurements and could be as great as 10% (Thompson et al., 2007c;
260 Worden et al., 2007).

261 A decade (2004-2014) of global ozonesonde data with locations shown in Figure 2, are utilized
262 in this study to validate our OMI ozone profile product. Most of our ozonesonde data were
263 obtained from the Aura Validation Data Center (AVDC) archive. It contains routine launches
264 from ozonesonde stations, mostly weekly and occasionally 2-3 times a week at some stations. It
265 also collects launches from field campaigns, for instance, IONS 06 (INTEX-B Ozone Network
266 Study 2006), ARCIONS (Arctic Intensive Ozonesonde Network Study)
267 (<http://croc.gsfc.nasa.gov/arcions/>) (Tarasick et al., 2010; Thompson et al., 2008). Data not
268 available at AVDC are obtained from other archives such as the World Ozone and Ultraviolet
269 Radiation Data Center (WOUDC) (<http://woudc.org/>), the Southern Hemisphere Additional
270 Ozonesondes (SHADOZ) (Thompson et al., 2007a; Thompson et al., 2007b), as well as archives
271 of recent field campaigns including DISCOVER-AQ (Deriving Information on Surface
272 Conditions from Column and Vertically Resolved Observations Relevant to Air Quality,
273 <http://discover-aq.larc.nasa.gov/>) (Thompson et al., 2015) and SEACR⁴S (Studies of Emissions

274 and Atmospheric Composition, Clouds and Climate Coupling by Regional Surveys,
275 <https://espo.nasa.gov/home/seac4rs>) (Toon et al., 2016). Almost all of the ozonesonde data in
276 this study were obtained from electrochemical concentration cell (ECC) ozonesondes, which is
277 based on the oxidation reaction of ozone with potassium iodide (KI) in solution. The exceptions
278 are Hohenpeissenberg station in Germany that uses Brewer-Mast (BM) ozonesondes, the New
279 Delhi, Poona, and Trivandrum stations that use Indian ozonesondes, and four Japanese stations
280 (i.e., Sapporo, Tsukuba, Naha and Syowa) that switched from KC ozonesondes to ECC
281 ozonesondes during late 2008 and early 2010. These types of ozonesondes have been reported to
282 have larger uncertainties than ECC ozonesondes (Hassler et al., 2014; Liu et al., 2013; WMO,
283 1998).

284 To avoid using anomalous profiles, we screen out ozonesondes that burst at pressure exceeding
285 200 hPa, ozone profiles with gaps greater than 3 km, more than 80 DU TOC or less than 100 DU
286 SOC. In the SOC comparison, we also filter measurements that do not reach 12 hPa. Some
287 ozonesonde data used in this paper (e.g. WOUDC data) are provided with a correction factor
288 (CF) derived by normalizing the integrated ozone column (appended with ozone climatology
289 above burst altitude) to the coincident total ozone column measured by a Dobson or Brewer
290 instrument to account for uncertainties mainly from the pump efficiency especially near the top
291 of the profiles. The CF is also included in our screening processes. If the CF is available, we
292 select ozonesonde profiles with the CF in the range of 0.85 to 1.15 to filter profiles that require
293 too much correction, and apply the correction. Finally, a small number of obviously erroneous
294 profiles are visually examined and rejected.

295 **3 Comparison Methodology**

296 Previous studies on the validation of satellite observations used a range of coincidence criteria.
297 Wang et al. (2011) set a 100 km radius and 3 hour time difference as coincidence criteria. Kroon
298 et al. (2011) applied coincidence criteria of $\pm 0.5^\circ$ for both latitude and longitude and 12 hours.
299 In this paper, we determine our coincident criteria based on the balance between finding most
300 coincident OMI/ozonesonde pairs to minimize differences due to spatiotemporal samplings and
301 finding a sufficient number of pairs for statistical analysis. For each screened ozonesonde profile,
302 we first select all filtered OMI data within $\pm 1^\circ$ latitude, $\pm 3^\circ$ longitude and ± 6 hours and then

303 find the nearest OMI retrieval within 100 km from the ozonesonde station to perform the
304 validation on the individual profile basis.

305 Ozonesondes have much finer vertical resolution than OMI retrievals. To account for the
306 different resolutions, ozonesonde profiles are first integrated into the corresponding OMI vertical
307 grids and then degraded to the OMI vertical resolution by using the OMI retrieval Averaging
308 Kernels (AKs) and *a priori* ozone profile based on the following equation:

$$309 \quad \hat{x} = x_a + A(x - x_a), \quad (1)$$

310 where x is the ozonesonde profile integrated into the OMI grid, \hat{x} is the retrieved ozone profile if
311 the ozonesonde is observed by OMI, A is the OMI AK matrix, and x_a is the OMI *a priori* ozone
312 profile. We refer to this retrieval as “convolved ozonesonde profile”, which is a reconstruction of
313 ozonesonde profile with OMI retrieval vertical resolution and sensitivity. Missing ozone profiles
314 above ozonesonde burst altitude are filled with OMI retrievals. The convolution process
315 essentially removes OMI smoothing errors and the impacts of *a priori* from the comparison so
316 that OMI/ozonesonde differences are mainly due to OMI/ozonesonde measurement precision,
317 spatiotemporal sampling differences and other errors. However, in the regions and altitudes
318 where OMI has low retrieval sensitivity, the comparisons can show good agreement because
319 both the retrieval and convolved ozonesonde approach the *a priori* profile. To overcome the
320 limitation of such a comparison, we also compare with unconvolved ozonesonde profiles since it
321 indicates how well the retrievals can represent the actual ozonesonde observations (i.e.,
322 smoothing errors are included as part of retrieval errors). In addition, we also compare OMI *a*
323 *priori* and convolved/unconvolved ozonesonde profiles to indicate the retrieval improvement
324 over the *a priori*.

325 For consistent calculations of TOC and SOC from the OMI/ozonesonde data, the tropopause
326 pressure included in the OMI retrieval and ozonesonde burst pressure (required to be less than 12
327 hPa or above ~30 km) are used as the proper boundaries. The TOC is integrated from the surface
328 to the tropopause. And the SOC is not the total stratospheric ozone column, but the ozone
329 column integrated from the tropopause pressure to the ozonesonde burst pressure.

330 The relative profile difference is calculated as (OMI- Sonde) / OMI *a priori* ×100% in the present
331 comparison with ozonesonde and with MLS in the companion paper. Choosing OMI *a priori*

332 rather than MLS/ozonesonde is to avoid unrealistic statistics skewed by extremely small values
333 in the reference data especially in the MLS retrievals of upper troposphere and lower
334 stratosphere ozone (Liu et al., 2010a). Unlike the profile comparison, ozonesonde/OMI
335 SOC/TOC values are used in the denominator in the computation of relative difference. To
336 exclude remaining extreme outliers in the comparison statistics, values that are exceeding 3σ
337 from the mean differences are filtered.

338 After applying the OMI/ozone filtering and coincident criteria, approximately 10,500
339 ozonesonde profiles are used in the validation. We performed the comparison for five latitude
340 bands: northern high latitudes (60° N- 90° N), northern mid-latitudes (30° N- 60° N), tropics (30°
341 S- 30° N), southern mid-latitudes (60° S- 30° S), and southern high latitudes (90° S- 60° S) to
342 understand the latitudinal variation of the retrieval performance. We investigated the seasonal
343 variations of the comparisons mainly at northern mid-latitudes where ozone retrieval shows
344 distinct seasonality and there are adequate coincidence pairs. To investigate the RA impacts on
345 OMI retrievals, we contrasted the comparison before (2004-2008, i.e., pre-RA) and after (2009-
346 2014, i.e., post-RA). Although we filter OMI data based on cloud fraction, cross-track position,
347 and SZA in the final evaluation of our retrievals against ozonesonde observations as shown in
348 Sect. 4.1.1., we conduct the comparison as a function of these parameters using coincidences at
349 all latitude bands to show how these parameters affect the retrieval quality as shown in the Sects.
350 4.1.2 – 4.1.4. In these evaluations, the filtering of OMI data based on cloud fraction, cross-track
351 position, and SZA are switched off, respectively. Approximately 15,000 additional ozonesonde
352 profiles are used in this extended evaluation. To evaluate the long-term performance of our
353 ozone profile retrievals, we analyze the monthly mean biases (MBs) of the OMI/ozonesonde
354 differences as a function of time using coincidences in the 60° S- 60° N region and then derive a
355 linear trends over the entire period as well as the pre-RA and post-RA periods.

356 **4 Results and Discussions**

357 **4.1 Comparison of Ozone sonde and OMI profiles**

358 **4.1.1 Ozone Profile Differences**

359 Comparisons of ozone profiles between OMI/a priori and ozonesondes with and without
360 applying OMI AKs for the 10-year period (2004-2014) are shown in the left panels of Figure 3.
361 The MBs and SDs vary spatially with altitude and latitude. Vertically, the SD typically
362 maximizes in the upper troposphere and lower stratosphere (UTLS) in all latitude bands due to
363 significant ozone variability and a priori uncertainty. Bak et al. (2013b) showed that the use of
364 Tropopause-Based (TB) ozone profile climatology with NCEP Global Forecast System (GFS)
365 daily tropopause pressure can significantly improve the a priori, and eventually reduce the
366 retrieval uncertainty. Consequently, the SDs of OMI/sonde differences in the UTLS at mid- and
367 high-latitudes can be reduced through reducing the retrieval uncertainties in a future version of
368 the algorithm that uses the TB climatology. Latitudinally, the agreement is better in the tropics
369 and becomes worse at higher latitudes. The patterns are generally similar in the northern and
370 southern hemispheres. The MBs between OMI and ozonesonde are within ~6% with AKs and
371 10% without AKs in the tropics and the middle latitudes. Large changes in the biases between
372 with and without AKs occur in the tropical troposphere where the bias differences reach 10%.
373 The MBs increase to 20-30% at high latitudes consistently with large oscillation from ~-20-30%
374 at ~300 hPa to +20% near the surface both with and without the application of AKs. At pressure
375 < 50 hPa, the SDs for comparisons with OMI AKs are typically 5-10% at all latitudes except for
376 the 90° S-60° S region. For pressure > 50 hPa, the SDs are within 18% and 27% in the tropics
377 and middle-latitudes, respectively, but increase to 40% at higher latitudes. The SDs for
378 comparison without applying OMI AKs, i.e., including OMI smoothing errors in the
379 OMI/ozonesonde differences, typically increase up to 5% for pressure < 50 hPa, but increase up
380 to 15-20% for pressure > ~50hPa. The smoothing errors derived from root square differences of
381 the MBs with and without OMI AKs are generally consistent with the retrieval estimate from the
382 optimal estimation.

383 The improvements of OMI over the climatological (a priori) profiles can be reflected in the
384 reduction of MBs and SDs in the comparisons between ozonesondes and OMI retrievals, and
385 between ozonesondes and a priori. The retrieval improvements in the MBs are clearly shown in
386 the tropics and at ~ 100 hPa pressure in the middle latitudes. At high latitudes, the MBs and
387 corresponding oscillations in the troposphere are much larger than these in the a priori
388 comparison, suggesting that these large biases are mainly caused by other systematic
389 measurements errors at high latitudes (larger SZAs and thus weaker signals). As can be seen
390 from the reduction of SDs, OMI retrievals show clear improvements over the a priori at pressure
391 < 300 hPa. For pressure > 300 hPa, the retrieval improvements vary with latitudes. There are
392 consistent retrieval improvements throughout the surface - 300hPa layer in the tropics and only
393 the 550 - 300 hPa layer at middle latitude, while there is no retrieval improvement over the a
394 priori for > 300 hPa at high latitudes. The failure to improve the retrieval over a priori in part of
395 the troposphere at middle and high latitudes is caused by several factors. They are the inherent
396 reduction in retrieval sensitivity to lower altitudes at larger SZAs as a result of reduced photon
397 penetration into the atmosphere, unrealized retrieval sensitivity arising from retrieval
398 interferences with other parameters (e.g., surface albedo) as discussed in Liu et al. (2010b) and
399 the use of floor-noise of 0.2% that underestimates the actual OMI measurement SNR. In
400 addition, the a priori ozone error in the climatology is quite small since the SDs of the
401 differences between the a priori and ozonesonde without AKs are typically less than 20% in the
402 lower troposphere for middle and high latitudes, which also makes it more difficult to improve
403 over the a priori comparison.

404 The right column of Figure 3 shows the comparisons between OMI retrievals and ozonesondes
405 convolved with OMI AKs in the pre-RA and post-RA periods, respectively. In the tropics and
406 mid-latitudes, the pre-RA comparison is better than the post-RA comparison, with SDs smaller
407 by up to ~8% at most altitudes especially in the troposphere. The pre-RA comparison also shows
408 smaller biases near ~300 hPa at middle latitudes while the post-RA comparison exhibits negative
409 biases reaching 8-12%. At high latitudes, the pre-RA period does not show persistent
410 improvement during the post-RA period. The pre-RA comparison shows slightly smaller SDs at
411 most altitudes and smaller negative biases by 10% around 300 hPa in the northern high latitudes,
412 and smaller positive biases by 20% near the surface in the southern high latitudes. The worse

413 results during the post-RA period are caused by increasingly noisy OMI measurements with
414 smaller SNR and the additional radiometric biases made by the RA, which vary with space and
415 time. The smaller SDs at some altitudes of high latitudes may reflect a combination of ozone
416 variation, uneven distribution of ozonesondes with varying uncertainty at different stations, and
417 cancellation of radiometric errors by the RA.

418 As seen from the number of OMI/ozonesonde coincidences shown in Figure 3, the northern mid-
419 latitudes and the tropics have sufficient coincidences to validate the retrievals as a function of
420 season. In the tropics, the retrieval comparison does exhibit little seasonality as expected (not
421 shown). Figure 4 shows the comparison similar to Figure 3(c) for each individual season at
422 northern middle latitudes. The comparison results are clearly season-dependent with different
423 altitude-dependent bias patterns, and with the smallest SDs in the summer (except for the MBs)
424 and the worst SDs in the winter. This indicates the general best retrieval sensitivity to lower
425 tropospheric ozone during the summer as a result of small SZAs and stronger signals and worst
426 retrieval sensitivity during the winter as a result of large SZAs and weaker signals. The MBs for
427 with and without AKs at 300 hPa vary from ~12% in the winter to -10% in the summer. The
428 overall MBs are the smallest during the spring, within 6%; but the MBs at pressure < 50 hPa are
429 the best during the summer. The maximum SDs vary from 31% in the winter to 20% in the
430 summer. Also, the retrieval in the summer shows the most improvements in terms of reduction in
431 SDs over the a priori in the lower troposphere at all tropospheric layers except for the bottom
432 layer, while the retrievals during other seasons show the improvement over a priori only above
433 the lowermost two/three layers. The seasonal variation of retrieval quality is partially caused by
434 the seasonal variations of the retrieval sensitivity and ozone variability. Bak et al. (2013b)
435 showed that the use of TB ozone climatology with daily NCEP GFS tropopause pressure can
436 significantly reduce the seasonal dependence of the comparison with ozonesondes. In addition,
437 radiometric calibration errors such as those caused by stray light and RA also contribute to the
438 seasonal variation of retrieval quality.

439 **4.1.2 Solar Zenith Angle Dependence**

440 The SZA of low earth orbit (LEO) satellite observation varies latitudinally and seasonally;
441 therefore the SZA dependence of the retrieval can cause latitudinal and seasonal dependent

442 retrieval biases. SZA is one of the main drivers that affect retrieval sensitivity especially to
443 tropospheric ozone. At large SZA, the measured backscattered signal becomes weak due to weak
444 incoming signal and long path length; the retrieval sensitivity to the tropospheric ozone
445 decreases due to reduced photon penetration to the troposphere. In addition, measurements are
446 subject to relatively larger radiometric errors such as those from stray light and as a result of
447 weaker signal, and radiative transfer calculations can lose accuracy at larger SZA (Caudill et al.,
448 1997).

449 Figure 5 gives the MBs and SDs of differences between OMI and ozonesondes (with OMI AKs)
450 in a function of SZAs. We can see that retrieval performance generally becomes worse at large
451 SZA. The SD typically increases with SZA especially at pressure > 300 hPa. At SZA larger than
452 75°, the SD at ~300 hPa increases to greater than ~45%. The variation of MBs with SZA is more
453 complicated. We see generally larger positive biases at larger SZA in the troposphere with >
454 20% biases at SZA larger than 75°. The MBs near ~ 30 hPa becomes more negative at larger
455 SZAs. There is a strip of positive biases of ~10% that slightly decreases in pressure from ~50
456 hPa at low SZA to ~10 hPa at large SZA; it might be due to some systematic radiometric biases
457 that can affect ozone at different altitudes varying with SZA. Because of the clear degradation of
458 the retrieval quality at large SZA, we set the SZA filtering threshold of 75° to filter OMI data.

459 **4.1.3 Cloud Fraction Dependence**

460 The presence of cloud affects retrieval sensitivity since clouds typically reduce sensitivity to
461 ozone below clouds and increase sensitivity to ozone above clouds. The accuracy of ozone
462 retrievals is sensitive to the uncertainties of cloud information and cloud treatment (Antón and
463 Loyola, 2011; Bak et al., 2015; Liu et al., 2010a). Our OMI ozone algorithm assumes clouds as
464 Lambertian surfaces with optical centroid cloud pressure from the OMI Raman cloud product
465 (Vasilkov et al., 2008), and partial clouds are modeled using independent pixel approximation
466 such that the overall radiance is the sum of clear and cloudy radiances weighted by the effective
467 cloud fraction. The cloud albedo is assumed to be 80% and is allowed to vary (>80%) with the
468 effective cloud fraction.

469 Figure 6 gives the influences of effective cloud fraction on the comparisons between OMI and
470 ozonesonde observations convolved with OMI AKs. The MBs and SDs do not change much with

471 cloud fraction for pressure < 100 hPa, and typically increase with the increase of cloud fraction
472 for pressure > 100 hPa. The MBs at pressure > 100 hPa, especially greater~300 hPa, increase to
473 more than 10% with cloud fraction greater than ~0.3. This indicates that the cloud fractions have
474 small impacts on the stratospheric retrievals but large impacts on the tropospheric retrievals as
475 expected. Some of the variation with cloud fraction such as negative biases near ~300 hPa at
476 cloud fraction of ~0.4 and the decreases of positive biases at ~ 50 hPa for cloud fraction greater
477 than ~0.8 may be partially related to the uncertainties of the cloud parameters. The chosen
478 filtering threshold of 0.3 in cloud fraction is a tradeoff between validating OMI data with
479 adequate retrieval sensitivity to tropospheric ozone and finding adequate number of
480 OMI/ozonesonde coincidences.

481 **4.1.4 Cross-Track Position Dependence**

482 The OMI swath is divided into 30 cross-track pixels at the UV1 spatial resolution of our product.
483 Each cross-track position is measured by a different part of the CCD detector, i.e., essentially a
484 different instrument. Radiometric calibration coefficients of the instrument are characterized
485 during pre-launch only at selected CCD column pixels and then interpolated to other columns,
486 causing variation in the radiometric calibration performance across the CCD detector. This in
487 turn causes cross-track dependent biases in the calibrated radiance (Liu et al., 2010b), which
488 therefore causes striping in almost all the OMI data products if no de-striping procedure is
489 applied. Our retrieval algorithm has included a first-order empirical correction independent of
490 space and time to remove the cross-track variability (Liu et al., 2010b). However, residual
491 dependence on cross-track position remains and the radiometric calibration at different position
492 can degrade differently with time (e.g., the RA impact). In addition, the viewing zenith angle
493 ranges from ~0° to ~70° and the footprint area increases by approximately an order of magnitude
494 from nadir to the first/last position. So the varying viewing zenith angle causes the variation of
495 retrieval sensitivities and atmospheric variabilities within varying footprint areas may also cause
496 additional cross-track dependence in the retrieval performance.

497 Figure 7 provides the MBs and SDs of the differences between OMI and ozonesonde convolved
498 with OMI AKs as a function of cross-track position for pre-RA and post-RA periods,
499 respectively. It clearly exhibits cross-track dependence especially with large positive/negative

500 MBs and large SDs at the first/last several extreme off-nadir positions. This is why we select
501 cross-track positions of 4-27 in the validation to avoid positions with large biases. The enhanced
502 biases/SDs at positions 24 (RA flagging not applied) and 27 (flagged as RA in UV2 since June
503 25, 2007 but not flagged/applied in UV1) are due to the RA impact during the post-RA period.
504 Cross-track positions 1-10 show consistent bias patterns with negative biases in ~300- 50 hPa
505 layer and positive biases in ~surface – 300 hPa layer, and large standard deviation around ~ 300
506 hPa although the magnitude decreases with increasing cross-track position. This pattern occurs
507 during both pre-RA and post-RA periods although the values are larger during the post-RA
508 period. For other cross-track positions, the variation is relatively smaller but we can still see
509 small striping patterns.

510 **4.2 Comparison of Partial Ozone Columns**

511 We investigate and validate OMI partial ozone columns, including SOCs, TOCs, and surface-
512 550 hPa and surface-750 hPa ozone columns in this section. We define the lowermost one and
513 two layer as surface-750 hPa and surface-550 hPa in this paper, respectively, for conveniences.
514 Similarly, we also analyze the validation results of SOCs and TOCs during pre-RA and post-RA,
515 respectively, to test the impacts of RA on OMI partial ozone columns. In addition, we validate
516 ozone columns from the surface to ~550 hPa (bottom two layers) and ~ 750 hPa (bottom one
517 layer) against ozonesonde observations in the tropics and mid-latitude summer where there is
518 better retrieval sensitivity to these quantities.

519 **4.2.1 Comparison of Stratospheric Ozone Columns (SOCs)**

520 The left column of Figure 8 shows the MBs and SDs of the comparisons of OMI and ozonesonde
521 SOCs for each of the five latitude bands during 2004-2014. In all regions, the OMI SOCs have
522 excellent agreement with ozonesonde SOCs regardless of whether ozonesonde data are
523 convolved with OMI AKs. The application of OMI AKs to ozonesonde SOCs only slightly
524 improves the comparison statistics. The MBs with OMI AKs are within 1.8% except for a
525 negative bias of 3% at northern high latitudes, while the SDs are within 5.1% except for 5.7% at
526 high latitudes. The correlation coefficient is greater than 0.95 except for 0.90 in the tropics due to
527 the smaller SOC range. The SDs are typically larger than the comparisons with MLS data (Liu et

528 al., 2010a) due to worse coincidence criteria, relatively larger uncertainty in the ozonesonde
529 stratospheric ozone columns compared to MLS data, and different altitude ranges of integration.

530 The middle and right columns of Figure 8 show comparison results during the pre-RA and post-
531 RA periods, respectively. The comparison is typically better during the pre-RA with SDs smaller
532 by 0.2-0.6% and larger correlation coefficients although the MBs are generally smaller during
533 the post-RA period. One exception is at southern high-latitudes where the post-RA comparison
534 statistics are significantly better except for the MB, consistent with Figure 3, likely due to a
535 combination of ozone variation between these two periods, uneven distribution of ozonesondes
536 at different stations, and cancellation of various calibration errors.

537 **4.2.2 Comparison of Partial Ozone Columns in the Troposphere**

538 The left column of Figure 9 shows the comparison of OMI and ozonesonde (with and without
539 OMI AKs) TOCs for each of the five latitude bands during 2004-2014. Without applying OMI
540 AKs, the MBs are within 1-3% except for 9% at northern high latitudes; The SDs are within 20%
541 in the tropics and mid-latitudes and increase to ~30-40% at high-latitudes. The correlation
542 coefficient ranges from 0.83 in the tropics to ~0.7 at middle latitudes, and 0.5-0.6 at high-
543 latitudes. The linear regression slopes are in the range 0.6-0.8 typically smaller at high latitudes
544 due to reduced retrieval sensitivity to the lower troposphere. After applying the OMI AKs to
545 ozonesonde data to remove smoothing errors, we see significant improvement in the comparison
546 statistics except for MBs, which are within 6% at all latitudes. The SDs are reduced to within
547 15% in the tropics and middle latitudes and ~30% (5.5-8.1 DU) at high latitudes; the correlation
548 improves by 0.04-0.12 and the slope significantly increases by 0.12-0.23 to the range 0.8-1.0 at
549 different latitude bands due to accounting for inadequate retrieval sensitivity to the lower and
550 middle troposphere.

551 The middle and right columns of Figure 9 show comparisons during pre-RA and post-RA,
552 respectively. The comparison between OMI and ozonesondes with OMI AKs TOCs during the
553 pre-RA period is significantly better than these during the post-RA period in the tropics and mid-
554 latitudes with SDs smaller by 3.4-5.5% and greater correlation. The MBs during the post-RA
555 period is smaller by ~2 DU at mid-latitudes, but larger by ~1 DU in the tropics. However, the

556 post-RA comparison is similar to the pre-RA comparison at northern high-latitudes and is even
557 better at southern high latitudes probably due to the aforementioned ozonesonde issues.

558 Figure 10 shows examples of time series when comparing individual OMI and ozonesondes
559 (with OMI AKs) TOCs and their corresponding differences at six selected stations, one for each
560 latitude region of 90° N-60° N, 60° N-30° N, 30° N-0°, 0°-30° S, 30° S-60° S and 60° S-90° S.
561 OMI TOC shows good agreement with ozonesondes at these stations with overall MBs ≤ 3 DU
562 and SDs less than 5.1 DU. The comparison is also good even in the high latitude regions partially
563 because the Summit and Neymayer stations only have ozonesonde launches during local
564 summer. Seasonal dependent biases are clearly seen at Payerne, and bias trends can be seen at
565 several stations with positive trends at Summit and Neumayer and a negative trend at Naha. In
566 the pre-RA and post-RA periods, the MBs are typically within 2 DU and the SDs are typically
567 smaller during the pre-RA period except for Naha. The better comparison (both mean bias and
568 standard deviation) during the post-RA period at Naha is likely due to the switch to ECC
569 ozonesondes beginning on November 13, 2008 from KC ozonesonde that have greater
570 uncertainty (WMO, 1998).

571 Figure 2 also shows the MBs and SDs of the TOC differences between OMI and ozonesonde
572 convolved with OMI AKs at each station/location where there are at least 10 coincident
573 OMI/ozonesonde pairs. OMI data generally exhibit good agreement with ozonesondes at most of
574 the stations, with MBs of ≤ 3 DU and SDs of ≤ 6 DU. In the tropics (30° S-30° N), very large
575 SDs (>11 DU) occur at the two Indian stations (New Delhi, and Trivandrum). In addition, there
576 is a large bias of > 6 DU at New Delhi. The poor comparisons at these two stations are likely
577 associated with the large uncertainties of the Indian ozonesonde data. Hilo has large biases of
578 ~ 4.5 DU with 3.2 and 6.2 DU for pre-RA and post-RA, respectively. Java also has a large bias of
579 ~ 5 DU but shows little difference between pre-RA and post-RA. Consistent $\sim 2\%$ and $\sim 5\%$
580 underestimates of OC by ozonesondes compared to OMI total ozone are found in Hilo and Java,
581 respectively (Thompson et al., 2012). These OC underestimates may partly explain the large
582 TOC biases in Hilo and Java. However, the reason for underestimates of ozonesonde-derived OC
583 is unknown. In the middle latitudes, noticeably large SDs and/or biases occur at a few stations
584 such as Churchill, Sable Islands, Hohenpeissenberg, and Parah. Three Japanese stations,
585 Sapporo, Tateno, and Naha, exhibit relatively large biases of 2-3 DU and even larger biases

586 before switching from KC to ECC sondes. Almost half of the 11 northern high latitude stations
587 (60° N- 90° N) and two of the 6 southern high-latitude stations have large SDs/biases. In addition
588 to retrieval biases from the OMI data, some of the large biases or SDs might be partially related
589 to ozonesonde type with different biases and uncertainties due to different types (e.g., Indian
590 sonde stations, Brewer-Mast ozonesonde at Hohenpeissenberg, three KC sonde stations),
591 manufacturers (e.g., SP vs. ENSCI for ECC sonde), sensor solution or related to individual sonde
592 operations, which was shown in the validation of GOME ozone profile retrievals (Liu et al.,
593 2006a).

594 Figure 11 shows the comparison for each season at northern mid-latitudes. Consistent with
595 profile comparison, the TOC comparison is season-dependent. When applying OMI AKs, the
596 mean bias varies from 3 DU in winter to -1.5 DU in summer. The SDs are within 6.8 DU with
597 the smallest value during fall due to less ozone variability. The regression slopes are very close,
598 within 0.04 around 0.67. The retrieval sensitivity is smallest during the summer as seen from the
599 greatest correlation and slope and relatively small standard deviation, and is the worst during the
600 winter. With OMI AKs applied to ozonesonde profiles, the MBs only slightly change (varying
601 from 3.5 DU to -1.3 DU), but the SDs are significantly reduced to within 5.2 DU, the slopes
602 significantly increase by ~ 0.2 to 0.8-1.0, and the correlation improves significantly during the
603 winter and spring.

604 Figure 12 compares the surface- ~ 550 hPa and surface- ~ 750 hPa ozone columns with ozonesonde
605 data in the middle latitudes during summer and the tropics. Compared to the TOC comparisons
606 in Figure 9 and Figure 11, the comparisons of these lower tropospheric ozone columns exhibit
607 smaller regression slopes and correlations that are a result of reduced retrieval sensitivity. In the
608 tropics, the slopes decrease from 0.78 in TOC to 0.65 in the surface- ~ 550 hPa ozone column and
609 ~ 0.50 in the surface- ~ 750 hPa column, with corresponding correlation from 0.83 to 0.74 in the
610 surface- ~ 550 hPa column, and 0.66 in the surface- ~ 750 hPa column. This indicates that the
611 retrievals in the surface- ~ 550 hPa/ ~ 750 hPa can capture $\sim 65\%/50\%$ of the actual ozone change
612 from the a priori. During the middle latitude summer, the slope decreases from 0.71 in the TOC
613 comparisons to 0.42 in the surface- ~ 550 hPa comparisons and 0.32 in the surface- ~ 750 hPa
614 comparisons, with corresponding correlation coefficients from 0.74 to 0.5 and 0.46. Thus, the
615 retrievals in the surface- ~ 550 hPa and ~ 750 hPa only capture $\sim 40\%/30\%$ of the actual ozone

616 change from the a priori. The MBs are generally small within 0.5 DU (5%) with SDs of ~3.6 DU
617 (20-28%) in the surface~550 hPa ozone column and ~2.5 DU (25-36%) in the surface~750 hPa
618 ozone column. After applying OMI AKs to account for inadequate retrieval sensitivity and
619 removing smoothing errors, the slope significantly increases to approach 1 (as expected). SDs
620 are reduced to ~10% in the middle latitudes and ~15% in the tropics.

621 **4.3 Evaluation of Long-term Performance**

622 Comparisons in Sects 4.1 and 4.2 indicated systematic differences between pre-RA and post-RA
623 periods and generally worse performance during the post-RA periods. To further illustrate the
624 long-term stability of our ozone profile product and understand the quality of OMI radiometric
625 calibration as a function of time, we analyze monthly MBs of OMI/ozonesonde differences with
626 OMI retrieval AKs in ozone profiles, SOCs, and TOCs. Due to the lack of OMI observations
627 during some months at high-latitudes, we focus the evaluation by using coincidence pairs in 60°
628 S-60° N. Monthly MBs are calculated only if there are more than 5 OMI-ozonesonde pairs in a
629 given month. Linear regression trend is on the MBs for the entire period (2004-2014) and/or for
630 the pre-RA and post-RA periods, respectively. The trend is considered statistically significant if
631 its P value is less than 0.05.

632 The linear trends of monthly mean ozone biases for each OMI layer between 60° S-60° N are
633 plotted in Figure 13 for each of the three periods. During 2004-2014, marked in black, ozone
634 biases at layers above 50.25 hPa show significant positive trends of 0.06-0.17 DU/year (0.17-
635 0.52%/year), while ozone biases between 290 hPa and 110 hPa exhibit significant negative
636 trends of 0.1-0.19 DU/year (1-2%/year). The positive trends in the stratosphere are generally
637 consistent with those shown in OMI-MLS comparisons (Huang et al., 2017). In the lowermost
638 three OMI layers, ozone differences are more stable but with several large spikes during the post-
639 RA periods likely due to the RA evolution or instrument operation. The derived trends for the
640 pre-RA period are generally more flat and insignificant at all layers indicating good stability of
641 our product as well as the OMI radiometric calibration. During the post-RA period, the derived
642 trends are positive above 75 hPa with statistical significance. These positive trends in the
643 stratosphere are generally similar to those over the entire period, suggesting the dominant
644 contribution of the post-RA period to the overall trend. In the altitude range 214 – 108 hPa, the

645 post-RA trends are also flat similar to the pre-RA trends, but the values are systematically
646 smaller during the post-RA period, causing significantly negative trends over the entire period.

647 The SOC biases exhibit small positive trend of 0.14 ± 0.09 DU/year in 2004-2014 with no
648 statistical significance (Figure 14(a)). This slight positive trend is a result of trend cancellation
649 by the positive trends above 80 hPa and negative trends between 220 hPa and 80 hPa. The TOC
650 biases reveal a significant negative trend of -0.18 ± 0.05 DU/year (Figure 14(b)), mostly from
651 layers in the upper troposphere. In the pre-RA and post-RA periods, both trends of both SOC and
652 TOC biases are relatively flat during the pre-RA period, while the SOC trend in the post-RA
653 period is 0.77 ± 0.20 DU/year with significance. It is noticeable that the P value of TOC trend in
654 the post-RA period is 0.06.

655 The significant trends of ozone biases at different layers as well as in SOC and TOC suggest that
656 the current ozone profile product is not suitable for trend studies especially during the post-RA
657 period. The relatively flat bias trends during the pre-RA periods and statistically significant
658 trends during the post-RA period confirm that the better stability of our product during the pre-
659 RA period and more temporal variation of the retrieval performance during the post-RA period
660 are likely associated with the RA evolution. In previous sections, the validation of our retrievals
661 revealed latitudinal/seasonal/SZA and cross-track dependent biases even during the pre-RA
662 period. This indicates the need to remove signal dependent errors and the calibration
663 inconsistency across the track. To maintain the spatial consistency and long-term stability of our
664 ozone profile product, we need to further improve OMI's radiometric calibration especially
665 during the post-RA period. Preferably, the calibration improvement should be done in the level
666 0-1b processing. If this option is not possible, we can perform soft calibration similar to Liu et al.
667 (2010b) but derive the correction as a function of time and latitude/SZA. In addition, it should be
668 noted that the trend calculation might be affected by factors such as the availability of correction
669 factors with ozonesondes (Morris et al., 2013), station-to-station variability and the uneven
670 spatiotemporal distribution of the ozonesondes, which can introduce considerable sampling
671 biases (Liu et al., 2009; Saunio et al., 2012).

672 **5 Summary and Conclusion**

673 We conducted a comprehensive evaluation of the quality of OMI ozone profile (PROFOZ)
674 products produced by the SAO algorithm, including their spatial consistency and long-term
675 performance using coincident global ozonesonde observations during the decade 2004-2014. To
676 better understand retrieval errors and sensitivity, we compared the retrieved ozone profiles and a
677 priori profile at individual layers with ozonesondes before and after being degraded to the OMI
678 vertical resolution with OMI retrieval average kernels (AKs). We also compared the integrated
679 SOC, TOC, and surface-~550/~750 hPa ozone columns with ozonesonde data. To understand the
680 spatial distribution of retrieval performance, the validations are grouped into five latitude ranges:
681 northern/southern high/middle latitudes, and the tropics. To investigate the impacts of the OMI
682 row anomaly (RA) on the retrievals, we contrasted the comparison before and after the
683 occurrence of major OMI RA in January 2009, i.e., pre-RA (2004-2008) and post-RA (2009-
684 2014) periods. In addition, we quantified the dependence of retrieval performance on seasonality
685 and several key parameters including solar zenith angle (SZA), cloud fraction, and cross-track
686 position. Finally, we analyzed the monthly mean variation of the mean biases (MBs) to examine
687 the long-term stability of the PROFOZ product.

688 The comparison between OMI and ozonesonde profiles varies in altitude, with maximum
689 standard deviations (SDs) in the Upper Troposphere and Lower Stratosphere (UTLS) due to
690 significant ozone variability, and varies with latitude similarly in the northern and southern
691 hemispheres. There is good agreement throughout the atmosphere in the tropics and mid-
692 latitudes. With the application of OMI AKs to ozonesonde data, the MBs are within 6%, and the
693 SDs increase from 5-10% for pressure < ~50 hPa to within 18%(27%) in the tropics/mid-
694 latitudes for pressure > ~50 hPa. In the high latitudes, the retrievals agree well with ozonesondes
695 only for pressure < ~50 hPa with MBs of < 10% and SDs of 5-15% for pressure < ~ 50 hPa, but
696 with MBs reaching 30% and SDs reaching 40% for pressure > ~50 hPa. The comparison results
697 are seasonally dependent. At northern mid-latitudes, there are generally the best retrieval
698 sensitivity and the smallest SDs as great as 20% in the summer, and the worst sensitivity and the
699 largest SDs reaching 31% in the winter. The MBs near 300 hPa vary from 12% in the winter to -
700 10% in the summer. The post-RA comparison is generally worse in the tropics and mid-latitudes
701 than the pre-RA comparison, with SDs larger by up to 8% in the troposphere and 2% in the

702 stratosphere, and with larger MBs around ~300 hPa in the mid-latitudes. But at high latitudes, the
703 pre-RA comparison does not show persistent improvement over the post-RA comparison, with
704 smaller biases and larger SDs at some altitudes, especially at southern high latitudes. The
705 retrieval improvement over a priori can be determined from the SD reduction of the retrieval
706 comparison from the a priori comparison. The retrievals demonstrate clear improvement over the
707 a priori down to the surface in the tropics, but only down to ~750 hPa during mid-latitude
708 summer, ~550 hPa during the other seasons of mid-latitudes and ~ 300 hPa at high latitudes.

709 Retrieval performance typically becomes worse at large SZA, especially at SZA larger than 75°,
710 where the MBs in the troposphere are >20% and the SDs near ~300 hPa are > 45%. The worse
711 performance at larger SZA is due to a combination of weaker signal and greater influence by
712 radiometric calibration errors such as due to stray light, and radiative transfer calculation errors.
713 The variation of SZA is likely responsible for the majority of the retrieval dependence on latitude
714 and season. The retrieval quality for pressure > ~100 hPa degrades with increasing cloudiness in
715 terms of MBs and SDs, with MBs greater than 10% at cloud fraction > 0.3. The retrieval
716 performance also varies with cross-track position, especially with large MBs and SDs at the
717 first/last extreme off-nadir positions (e.g., 1-3 and 28-30). The dependence is stronger during the
718 post-RA period.

719 The integrated SOCs and TOCs also exhibit good agreement with ozonesondes. With the
720 convolution of OMI AKs to ozonesonde data, the SOC MBs are within 2% with SDs within
721 ~5.1% in the tropics and mid-latitudes. These statistics do not change much even without the
722 applications of OMI AKs. The comparison becomes slightly worse at high latitudes, with MBs
723 up to 3% and SDs up to 6%. The pre-RA comparison is generally better with smaller SDs of 0.2-
724 0.6% except for southern high latitudes, although with slightly larger MBs. The TOC MBs and
725 SDs with OMI AKs are within 6%, with SDs of <~15% in the tropics and mid-latitudes but reach
726 30% at high latitudes. The pre-RA TOC comparison is also better in the tropics and mid-latitudes
727 with SDs smaller by 3.4-5.5% but worse values at southern high latitudes. The TOC comparison
728 at northern mid-latitudes varies with season, with MBs of 11%. There are worse correlation
729 during winter and MBs of -3% and best correlation in summer. The TOC comparison also shows
730 noticeable station-to-station variability in similar latitude ranges with much larger MBs and/or
731 SDs at the two Indian stations and larger MBs at several Japanese stations before they switched

732 from KC ozonesondes to ECC ozonesondes. This demonstrates the impacts of ozonesonde
733 uncertainties due to sonde types, manufacturers, sensor solution and operations. Without
734 applying OMI AKs, the TOC correlation with ozonesondes typically becomes worse at higher
735 latitudes, ranging from 0.83 in the tropics to 0.5-0.6 at high latitudes. The linear regression slope
736 is within 0.6-0.8, typically smaller at higher latitudes, reflecting the smaller retrieval sensitivity
737 down to the troposphere at higher latitudes mainly resulting from larger SZA. The convolution of
738 AKs significantly improves the correlation and slope. The impact of retrieval sensitivity related
739 to SZA is also reflected in the seasonal dependence of the comparison at mid-latitudes.

740 The surface-~550/750 hPa ozone columns in the tropics during mid-latitude summer compare
741 quite well with ozonesonde data, with MBs of < 5% and SDs of 20-25%/28-36% without OMI
742 AKs. The correlation and slope decrease with decreasing altitude range due to reduced retrieval
743 sensitivity down to the lower troposphere. These columns capture ~65%/50% of the actual ozone
744 change in the tropics and ~40%/30% in the troposphere. Convolution of ozonesonde data with OMI
745 AKs significantly increases the slope to ~1 and reduce the SDs to 10-15%.

746 The contrast of pre-RA and post-RA comparisons indicates generally worse post-RA
747 performance with larger SDs. Linear trend analysis of the OMI/ozonesonde monthly MBs further
748 reveals additional RA impact. The temporal performance over 60° S-60° N is generally stable
749 with no statistically significant trend during the pre-RA period, but displays a statistically
750 significant trend of 0.14-0.7%/year at individual layers for pressure < ~80 hPa, 0.7 DU/year in
751 SOC and -0.33 DU/year in TOC during the post-RA period. Because of these artificial trends in
752 our product, we caution against using our product for ozone trend studies.

753 This validation study demonstrates generally good retrieval performance of our ozone profile
754 product especially in the tropics and mid-latitudes during the pre-RA period. However, the
755 spatiotemporal variation of retrieval performance suggests that OMI's radiometric calibration
756 should be improved, especially during the post-RA period, including the removal of signal-
757 dependent errors, calibration inconsistency across the track and with time to maintain the long-
758 term stability and spatial consistency of our ozone profile product.

759 **Data Availability**

760 OMI PROFOZ (version 0.9.3) used in this study is available to users at Aura Validation Data
761 Center (AVDC) (<https://avdc.gsfc.nasa.gov/index.php?site=1389025893&id=74>).

762

763 **Acknowledgements**

764 This study was supported by the NASA Atmospheric Composition: Aura Science Team
765 (NNX14AF16G) and the Smithsonian Institution. The Dutch-Finnish OMI instrument is part of
766 the NASA EOS Aura satellite payload. The OMI Project is managed by NIVR and KNMI in the
767 Netherlands. We acknowledge the OMI International Science Team for producing OMI data. We
768 also acknowledge the ozonesonde providers and their funding agencies for making ozonesonde
769 measurements, and the Aura Validation Data Center (AVDC), WOUDC, SHADOZ,
770 DISCOVER-AQ, and SEACR⁴S for archiving the ozonesonde data.

Formatted: Heading 1

771 **References**

- 772 Antón, M., and Loyola, D.: Influence of cloud properties on satellite total ozone observations, *J.*
773 *Geophys. Res.*, 116, doi: 10.1029/2010JD014780, 2011.
- 774 Bak, J., Kim, J. H., Liu, X., Chance, K., and Kim, J.: Evaluation of ozone profile and
775 tropospheric ozone retrievals from GEMS and OMI spectra, *Atmos. Meas. Tech.*, 6, 239-249,
776 2013a.
- 777 Bak, J., Liu, X., Kim, J. H., Chance, K., and Haffner, D. P.: Validation of OMI total ozone
778 retrievals from the SAO ozone profile algorithm and three operational algorithms with Brewer
779 measurements, *Atmos. Chem. Phys.*, 15, 667-683, doi: 10.5194/acp-15-667-2015, 2015.
- 780 Bak, J., Liu, X., Wei, J. C., Pan, L. L., Chance, K., and Kim, J. H.: Improvement of OMI ozone
781 profile retrievals in the upper troposphere and lower stratosphere by the use of a tropopause-
782 based ozone profile climatology, *Atmos. Meas. Tech.*, 6, 2239-2254, doi: 10.5194/amt-6-2239-
783 2013, 2013b.
- 784 Bhartia, P. K., and Wellemeyer, C. G.: TOMS-V8 total ozone algorithm, in: *OMI Algorithm*
785 *Theoretical Basis Document*, edited by: Bhartia, P. K., Greenbelt, 2002.
- 786 Cai, Z., Liu, Y., Liu, X., Chance, K., Nowlan, C. R., Lang, R., Munro, R., and Suleiman, R.:
787 Characterization and correction of Global Ozone Monitoring Experiment 2 ultraviolet
788 measurements and application to ozone profile retrievals, *J. Geophys. Res.*, 117, doi:
789 10.1029/2011jd017096, 2012.
- 790 Caudill, T. R., Flittner, D. E., Herman, B. M., Torres, O., and McPeters, R. D.: Evaluation of the
791 pseudo-spherical approximation for backscattered ultraviolet radiances and ozone retrieval, *J.*
792 *Geophys. Res.*, 102, 3881-3890, 1997.
- 793 Claas, J.: *OMI and AURA: Status, Instrument, Spacecraft and Operations*, OMI Science Meeting
794 Meeting, De Bilt, the Netherlands, 2014.
- 795 Deshler, T., Mercer, J. L., Smit, H. G. J., Stubi, R., Levrat, G., Johnson, B. J., Oltmans, S. J.,
796 Kivi, R., Thompson, A. M., Witte, J., Davies, J., Schmidlin, F. J., Brothers, G., and Sasaki, T.:
797 Atmospheric comparison of electrochemical cell ozonesondes from different manufacturers, and
798 with different cathode solution strengths: The Balloon Experiment on Standards for
799 Ozonesondes, *J. Geophys. Res.*, 113, doi: 10.1029/2007JD008975, 2008.
- 800 Hassler, B., Petropavlovskikh, I., Staehelin, J., August, T., Bhartia, P. K., Clerbaux, C.,
801 Degenstein, D., Mazière, M. D., Dinelli, B. M., Dudhia, A., Dufour, G., Frith, S. M., Froidevaux,
802 L., Godin-Beekmann, S., Granville, J., Harris, N. R. P., Hoppel, K., Hubert, D., Kasai, Y.,
803 Kurylo, M. J., Kyrölä, E., Lambert, J. C., Levelt, P. F., McElroy, C. T., McPeters, R. D., Munro,
804 R., Nakajima, H., Parrish, A., Raspollini, P., Remsberg, E. E., Rosenlof, K. H., Rozanov, A.,
805 Sano, T., Sasano, Y., Shiotani, M., Smit, H. G. J., Stiller, G., Tamminen, J., Tarasick, D. W.,
806 Urban, J., van der A, R. J., Veefkind, J. P., Vigouroux, C., von Clarmann, T., von Savigny, C.,
807 Walker, K. A., Weber, M., Wild, J., and Zawodny, J. M.: Past changes in the vertical distribution
808 of ozone - Part 1: Measurement techniques, uncertainties and availability, *Atmos. Meas. Tech.*,
809 7, 1395-1427, doi: 10.5194/amt-7-1395-2014, 2014.

810 Hayashida, S., Liu, X., Ono, A., Yang, K., and Chance, K.: Observation of ozone enhancement
811 in the lower troposphere over East Asia from a space-borne ultraviolet spectrometer, *Atmos.*
812 *Chem. Phys.*, 15, 9865-9881, doi: 10.5194/acp-15-9865-2015, 2015.

813 Huang, G., Liu, X., Chance, K., Yang, K., and Cai, Z.: Validation of 10-year SAO OMI Ozone
814 Profile (PROFOZ) Product Using Aura MLS Measurements, *Atmos. Meas. Tech. Discuss.*,
815 2017, 1-25, doi: 10.5194/amt-2017-92, 2017.

816 Huang, G., Newchurch, M. J., Kuang, S., Buckley, P. I., Cantrell, W., and Wang, L.: Definition
817 and determination of ozone laminae using Continuous Wavelet Transform (CWT) analysis,
818 *Atmos. Environ.*, 104, 125-131, doi: 10.1016/j.atmosenv.2014.12.027, 2015.

819 Johnson, B. J.: Electrochemical concentration cell (ECC) ozonesonde pump efficiency
820 measurements and tests on the sensitivity to ozone of buffered and unbuffered ECC sensor
821 cathode solutions, *IEEE T. Geosci. Remote.*, 107, 4393, doi: 10.1029/2001jd000557, 2002.

822 Kim, P. S., Jacob, D. J., Liu, X., Warner, J. X., Yang, K., Chance, K., Thouret, V., and Nedelec,
823 P.: Global ozone-CO correlations from OMI and AIRS: constraints on tropospheric ozone
824 sources, *Atmos. Chem. Phys.*, 13, 9321-9335, doi: 10.5194/acp-13-9321-2013, 2013.

825 Kivi, R., Kyrö, E., Turunen, T., Harris, N. R. P., von der Gathen, P., Rex, M., Andersen, S. B.,
826 and Wohltmann, I.: Ozonesonde observations in the Arctic during 1989–2003: Ozone variability
827 and trends in the lower stratosphere and free troposphere, *J. Geophys. Res.*, 112, doi:
828 10.1029/2006JD007271, 2007.

829 Komhyr, W. D.: Operations on handbook-Ozone measurements to 40-km altitude with model 4A
830 electrochemical concentration cell (ECC) ozonesondes, NOAA Tech. Memo. ERLARL-149 Air
831 Resour. Lab., Boulder, CO, 49 pp., 1986.

832 Komhyr, W. D., Connor, B. J., McDermid, I. S., McGee, T. J., Parrish, A. D., and Margitan, J. J.:
833 Comparison of STOIC 1989 ground-based lidar, microwave spectrometer, and Dobson
834 spectrophotometer Umkehr ozone profiles with ozone profiles from balloon-borne
835 electrochemical concentration cell ozonesondes, *J. Geophys. Res.*, 100, 9273-9282, 1995.

836 Kroon, M., de Haan, J. F., Veeffkind, J. P., Froidevaux, L., Wang, R., Kivi, R., and Hakkarainen,
837 J. J.: Validation of operational ozone profiles from the Ozone Monitoring Instrument, *J.*
838 *Geophys. Res.*, 116, D18305, doi: 10.1029/2010jd015100, 2011.

839 Lal, S., Venkataramani, S., Srivastava, S., Gupta, S., Mallik, C., Naja, M., Sarangi, T., Acharya,
840 Y. B., and Liu, X.: Transport effects on the vertical distribution of tropospheric ozone over the
841 tropical marine regions surrounding India, *J. Geophys. Res.*, 118, 1513-1524, 2013.

842 Levelt, P. F., van den Oord, G. H. J., Dobber, M. R., Malkki, A., Visser, H., de Vries, J.,
843 Stammes, P., Lundell, J. O. V., and Saari, H.: The Ozone Monitoring Instrument, *IEEE T.*
844 *Geosci. Remote.*, 44, 1093-1101, 2006.

845 Liu, G., Liu, J., Tarasick, D. W., Fioletov, V. E., Jin, J. J., Moeini, O., Liu, X., Sioris, C. E., and
846 Osman, M.: A global tropospheric ozone climatology from trajectory-mapped ozone soundings,
847 *Atmos. Chem. Phys.*, 13, 10659-10675, doi: 10.5194/acp-13-10659-2013, 2013.

848 Liu, G., Tarasick, D. W., Fioletov, V. E., Sioris, C. E., and Rochon, Y. J.: Ozone correlation
849 lengths and measurement uncertainties from analysis of historical ozonesonde data in North
850 America and Europe, *J. Geophys. Res.*, 114, doi: 10.1029/2008JD010576, 2009.

851 Liu, X., Bhartia, P. K., Chance, K., Froidevaux, L., Spurr, R. J. D., and Kurosu, T. P.: Validation
852 of Ozone Monitoring Instrument (OMI) ozone profiles and stratospheric ozone columns with
853 Microwave Limb Sounder (MLS) measurements, *Atmos. Chem. Phys.*, 10, 2539-2549, doi:
854 10.5194/acp-10-2539-2010, 2010a.

855 Liu, X., Bhartia, P. K., Chance, K., Spurr, R. J. D., and Kurosu, T. P.: Ozone profile retrievals
856 from the Ozone Monitoring Instrument, *Atmos. Chem. Phys.*, 10, 2521-2537, doi: 10.5194/acp-
857 10-2521-2010, 2010b.

858 Liu, X., Chance, K., and Kurosu, T. P.: Improved ozone profile retrievals from GOME data with
859 degradation correction in reflectance, *Atmos. Chem. Phys.*, 7, 1575-1583, 2007.

860 Liu, X., Chance, K., Sioris, C. E., Kurosu, T. P., and Newchurch, M. J.: Intercomparison of
861 GOME, ozonesonde, and SAGE II measurements of ozone: Demonstration of the need to
862 homogenize available ozonesonde data sets, *J. Geophys. Res.*, 111, D114305, doi:
863 10.1029/2005jd006718, 2006a.

864 Liu, X., Chance, K., Sioris, C. E., Kurosu, T. P., Spurr, R. J. D., Martin, R. V., Fu, T.-M., Logan,
865 J. A., Jacob, D. J., Palmer, P. I., Newchurch, M. J., Megretskaja, I. A., and Chatfield, R. B.: First
866 directly retrieved global distribution of tropospheric column ozone from GOME: Comparison
867 with the GEOS-CHEM model, *J. Geophys. Res.*, 111, doi: 10.1029/2005JD006564, 2006b.

868 Liu, X., Chance, K., Sioris, C. E., Spurr, R. J. D., Kurosu, T. P., Martin, R. V., and Newchurch,
869 M. J.: Ozone profile and tropospheric ozone retrievals from the Global Ozone Monitoring
870 Experiment: Algorithm description and validation, *J. Geophys. Res.*, 110, D20307, doi:
871 10.1029/2005jd006240, 2005.

872 McPeters, R. D., Labow, G. J., and Logan, J. A.: Ozone climatological profiles for satellite
873 retrieval algorithms, *J. Geophys. Res.*, 112, D05308, doi: 10.1029/2005jd006823, 2007.

874 Morris, G. A., Labow, G., Akimoto, H., Takigawa, M., Fujiwara, M., Hasebe, F., Hirokawa, J.,
875 and Koide, T.: On the use of the correction factor with Japanese ozonesonde data, *Atmos. Chem.*
876 *Phys.*, 13, 1243-1260, doi: 10.5194/acp-13-1243-2013, 2013.

877 Pittman, J. V., Pan, L. L., Wei, J. C., Irion, F. W., Liu, X., Maddy, E. S., Barnet, C. D., Chance,
878 K., and Gao, R.-S.: Evaluation of AIRS, IASI, and OMI ozone profile retrievals in the
879 extratropical tropopause region using in situ aircraft measurements, *J. Geophys. Res.*, 114,
880 24109, doi: 10.1029/2009jd012493, 2009.

881 Saunio, M., Emmons, L., Lamarque, J. F., Tilmes, S., Wespes, C., Thouret, V., and Schultz, M.:
882 Impact of sampling frequency in the analysis of tropospheric ozone observations, *Atmos. Chem.*
883 *Phys.*, 12, 6757-6773, doi: 10.5194/acp-12-6757-2012, 2012.

884 Sellitto, P., Bojkov, B. R., Liu, X., Chance, K., and Del Frate, F.: Tropospheric ozone column
885 retrieval at northern mid-latitudes from the Ozone Monitoring Instrument by means of a neural
886 network algorithm, *Atmospheric Measurement Techniques*, 4, 2375-2388, 2011.

887 Smit, H. G. J., Straeter, W., Johnson, B. J., Oltmans, S. J., Davies, J., Tarasick, D. W., Hoegger,
888 B., Stubi, R., Schmidlin, F. J., Northam, T., Thompson, A. M., Witte, J. C., Boyd, I., and Posny,
889 F.: Assessment of the performance of ECC-ozonesondes under quasi-flight conditions in the
890 environmental simulation chamber: Insights from the Juelich Ozone Sonde Intercomparison
891 Experiment (JOSIE), *J. Geophys. Res.*, 112, 19306, 2007.

892 Tarasick, D. W., Jin, J. J., Fioletov, V. E., Liu, G., Thompson, A. M., Oltmans, S. J., Liu, J.,
893 Sioris, C. E., Liu, X., Cooper, O. R., Dann, T., and Thouret, V.: High-resolution tropospheric
894 ozone fields for INTEX and ARCTAS from IONS ozonesondes, *J. Geophys. Res.*, 115, 20301,
895 doi: doi: 10.1029/2009JD012918, 2010.

896 Thompson, A. M., Miller, S. K., Tilmes, S., Kollonige, D. W., Witte, J. C., Oltmans, S. J.,
897 Johnson, B. J., Fujiwara, M., Schmidlin, F. J., Coetzee, G. J. R., Komala, N., Maata, M., bt
898 Mohamad, M., Nguyo, J., Mutai, C., Ogino, S. Y., Da Silva, F. R., Leme, N. M. P., Posny, F.,
899 Scheele, R., Selkirk, H. B., Shiotani, M., Stubi, R., Levrat, G., Calpini, B., Thouret, V., Tsuruta,
900 H., Canossa, J. V., Vömel, H., Yonemura, S., Diaz, J. A., Tan Thanh, N. T., and Thuy Ha, H. T.:
901 Southern Hemisphere Additional Ozonesondes (SHADOZ) ozone climatology (2005-2009):
902 Tropospheric and tropical tropopause layer (TTL) profiles with comparisons to OMI-based
903 ozone products, *J. Geophys. Res.*, 117, doi: 10.1029/2011jd016911, 2012.

904 Thompson, A. M., Stauffer, R. M., Miller, S. K., Martins, D. K., Joseph, E., Weinheimer, A. J.,
905 and Diskin, G. S.: Ozone profiles in the Baltimore-Washington region (2006-2011): satellite
906 comparisons and DISCOVER-AQ observations, *J Atmos Chem*, 72, 393-422, doi:
907 10.1007/s10874-014-9283-z, 2015.

908 Thompson, A. M., Stone, J. B., Witte, J. C., Miller, S. K., Oltmans, S. J., Kucsera, T. L., Ross,
909 K. L., Pickering, K. E., Merrill, J. T., Forbes, G., Tarasick, D. W., Joseph, E., Schmidlin, F. J.,
910 McMillan, W. W., Warner, J., Hints, E. J., and Johnson, J. E.: Intercontinental Chemical
911 Transport Experiment Ozonesonde Network Study (IONS) 2004: 2. Tropospheric ozone budgets
912 and variability over northeastern North America, *J. Geophys. Res.*, 112, doi:
913 10.1029/2006jd007670, 2007a.

914 Thompson, A. M., Stone, J. B., Witte, J. C., Miller, S. K., Pierce, R. B., Chatfield, R. B.,
915 Oltmans, S. J., Cooper, O. R., Loucks, A. L., Taubman, B. F., Johnson, B. J., Joseph, E.,
916 Kucsera, T. L., Merrill, J. T., Morris, G. A., Hersey, S., Forbes, G., Newchurch, M. J.,
917 Schmidlin, F. J., Tarasick, D. W., Thouret, V., and Cammas, J.-P.: Intercontinental Chemical
918 Transport Experiment Ozonesonde Network Study (IONS) 2004: 1. Summertime upper
919 troposphere/lower stratosphere ozone over northeastern North America, *J. Geophys. Res.*, 112,
920 doi: 10.1029/2006jd007441, 2007b.

921 Thompson, A. M., Witte, J. C., Smit, H. G. J., Oltmans, S. J., Johnson, B. J., Kirchhoff, V. W. J.
922 H., and Schmidlin, F. J.: Southern Hemisphere Additional Ozonesondes (SHADOZ) 1998–2004
923 tropical ozone climatology: 3. Instrumentation, station-to-station variability, and evaluation with
924 simulated flight profiles, *J. Geophys. Res.*, 112, doi: 10.1029/2005jd007042, 2007c.

925 Thompson, A. M., Yorks, J. E., Miller, S. K., Witte, J. C., Dougherty, K. M., Morris, G. A.,
926 Baumgardner, D., Ladino, L., and Rappenglück, B.: Tropospheric ozone sources and wave
927 activity over Mexico City and Houston during MILAGRO/Intercontinental Transport

928 Experiment (INTEX-B) Ozonesonde Network Study, 2006 (IONS-06), *Atmos. Chem. Phys.*, 8,
929 5113-5125, 2008.

930 Toon, O. B., Maring, H., Dibb, J., Ferrare, R., Jacob, D. J., Jensen, E. J., Luo, Z. J., Mace, G. G.,
931 Pan, L. L., Pfister, L., Rosenlof, K. H., Redemann, J., Reid, J. S., Singh, H. B., Thompson, A.
932 M., Yokelson, R., Minnis, P., Chen, G., Jucks, K. W., and Pszenny, A.: Planning,
933 implementation, and scientific goals of the Studies of Emissions and Atmospheric Composition,
934 Clouds and Climate Coupling by Regional Surveys (SEAC4RS) field mission, *J. Geophys. Res.*,
935 121, 4967-5009, doi: 10.1002/2015jd024297, 2016.

936 van Oss, R. F., Voors, R. H. M., and Spurr, R. J. D.: Ozone profile algorithm, in: OMI Algorithm
937 Theoretical Basis Document, Volume II: OMI ozone products, edited by: Bhartia, P. K.,
938 Greenbelt, MD, 51-73, 2001.

939 Vasilkov, A., Joiner, J., Spurr, R., Bhartia, P. K., Levelt, P., and Stephens, G.: Evaluation of the
940 OMI cloud pressures derived from rotational Raman scattering by comparisons with other
941 satellite data and radiative transfer simulations, *J. Geophys. Res.-Atmos.*, 113, n/a-n/a, doi:
942 10.1029/2007JD008689, 2008.

943 Veefkind, J. P., de Haan, J. F., Brinksma, E. J., Kroon, M., and Levelt, P. F.: Total Ozone From
944 the Ozone Monitoring Instrument (OMI) Using the DOAS Technique, *IEEE T. Geosci. Remote.*,
945 44, 1239-1244, 2006.

946 Wang, L., Newchurch, M. J., Biazar, A., Liu, X., Kuang, S., Khan, M., and Chance, K.:
947 Evaluating AURA/OMI ozone profiles using ozonesonde data and EPA surface measurements
948 for August 2006, *Atmos. Environ.*, 45, 5523-5530, doi: 10.1016/j.atmosenv.2011.06.012, 2011.

949 WMO: SPARC/IO3C/GAW Assessment of trends in the vertical distribution of ozone,
950 GenevaRep. 43, 1998.

951 Worden, H. M., Logan, J. A., Worden, J. R., Beer, R., Bowman, K., Clough, S. A., Eldering, A.,
952 Fisher, B. M., Gunson, M. R., Herman, R. L., Kulawik, S. S., Lampel, M. C., Luo, M.,
953 Megretskaya, I. A., Osterman, G. B., and Shephard, M. W.: Comparisons of Tropospheric
954 Emission Spectrometer (TES) ozone profiles to ozonesondes: Methods and initial results, *J.*
955 *Geophys. Res.*, 112, doi: 10.1029/2006jd007258, 2007.

956 Yang, Q., Cunnold, D. M., Wang, H. J., Froidevaux, L., Claude, H., Merrill, J., Newchurch, M.,
957 and Oltmans, S. J.: Midlatitude tropospheric ozone columns derived from the Aura Ozone
958 Monitoring Instrument and Microwave Limb Sounder measurements, *J. Geophys. Res.: Atmos.*,
959 112, D20305, doi: 10.1029/2007JD008528, 2007.

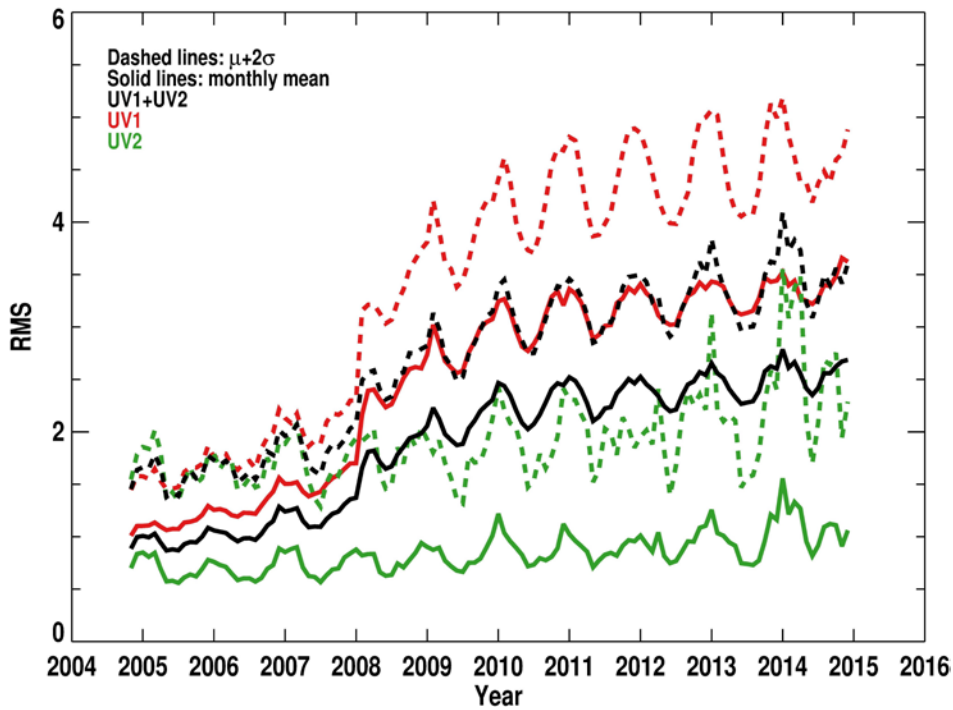
960 Ziemke, J. R., Olsen, M. A., Witte, J. C., Douglass, A. R., Strahan, S. E., Wargan, K., Liu, X.,
961 Schoeberl, M. R., Yang, K., Kaplan, T. B., Pawson, S., Duncan, B. N., Newman, P. A., Bhartia,
962 P. K., and Heney, M. K.: Assessment and applications of NASA ozone data products derived
963 from Aura OMI/MLS satellite measurements in context of the GMI chemical transport model, *J.*
964 *Geophys. Res.*, 119, 5671-5699, doi: 10.1002/2013jd020914, 2014.

965

966

967 **Figures and Figure Captions**

968

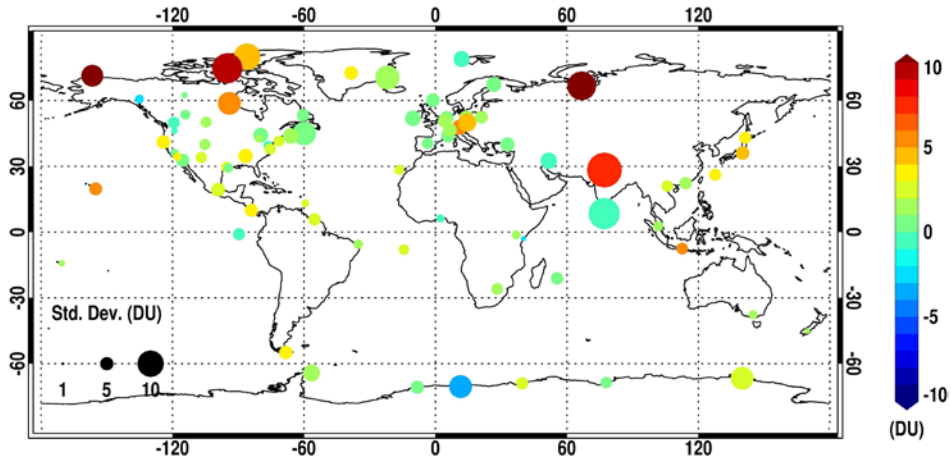


969

970 **Figure 1** Variation of monthly mean OMI RMS (defined as Root Mean Square of the ratio of
971 radiance residuals to assumed radiance errors). The dashed and solid lines represent respectively
972 the monthly mean RMS, and the sum of monthly mean plus its two standard deviations that is set
973 as the RMS threshold for data screening.

974

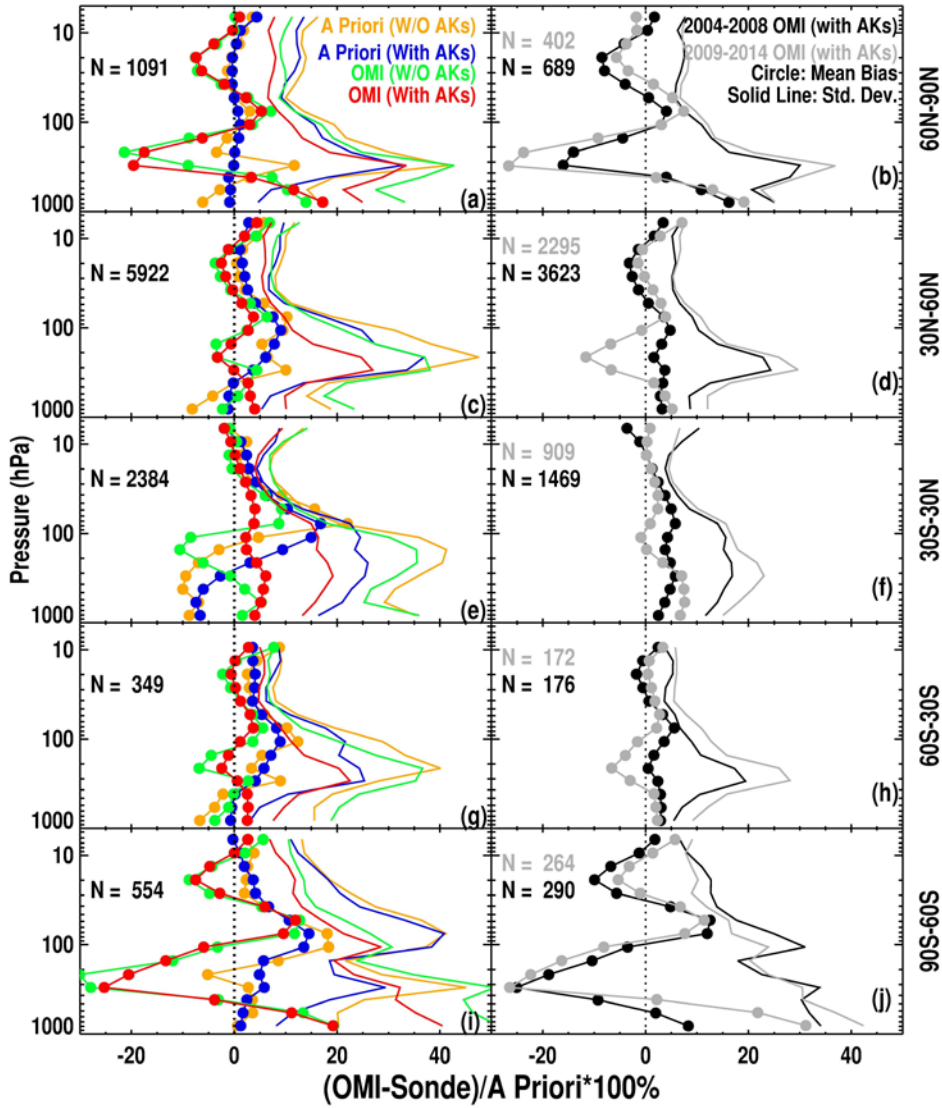
975



976

977 **Figure 2** The distribution of ozonesonde stations in this study. The color represents the mean biases
978 between OMI and ozonesonde tropospheric ozone columns (TOCs) at each station (if the number of
979 OMI and ozonesonde pairs is more than 10), and the dot size represents the standard deviation.

980



982

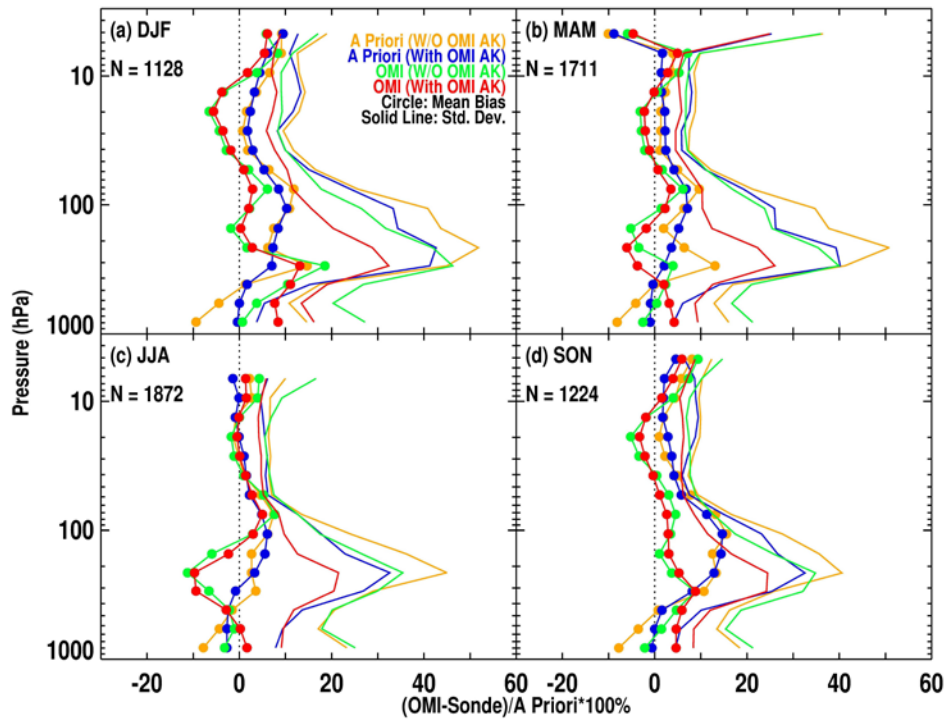
983 Figure 3 Mean relative biases in ozone (line with circles) and corresponding standard deviations
 984 (solid lines) between OMI retrieval/a priori and ozonesondes with and without applying OMI
 985 retrieval averaging kernels (i.e., with AKs, and W/O AKs in red and green for comparing retrievals

986 and in blue and yellow for comparing a priori) for five different latitude bands. The left panels
987 show the comparison using 10 years of OMI data (2004-2014), and the right panels show the
988 comparison between OMI retrieval and ozonesonde with OMI AKs for before and after the
989 occurrence of serious OMI row anomaly (RA), i.e., pre-RA (2004-2008) in black and post-RA
990 (2009-2014) in gray, respectively. The number (N) of OMI/ozonesonde coincidences used in the
991 comparison is indicated in the legends.

992

993

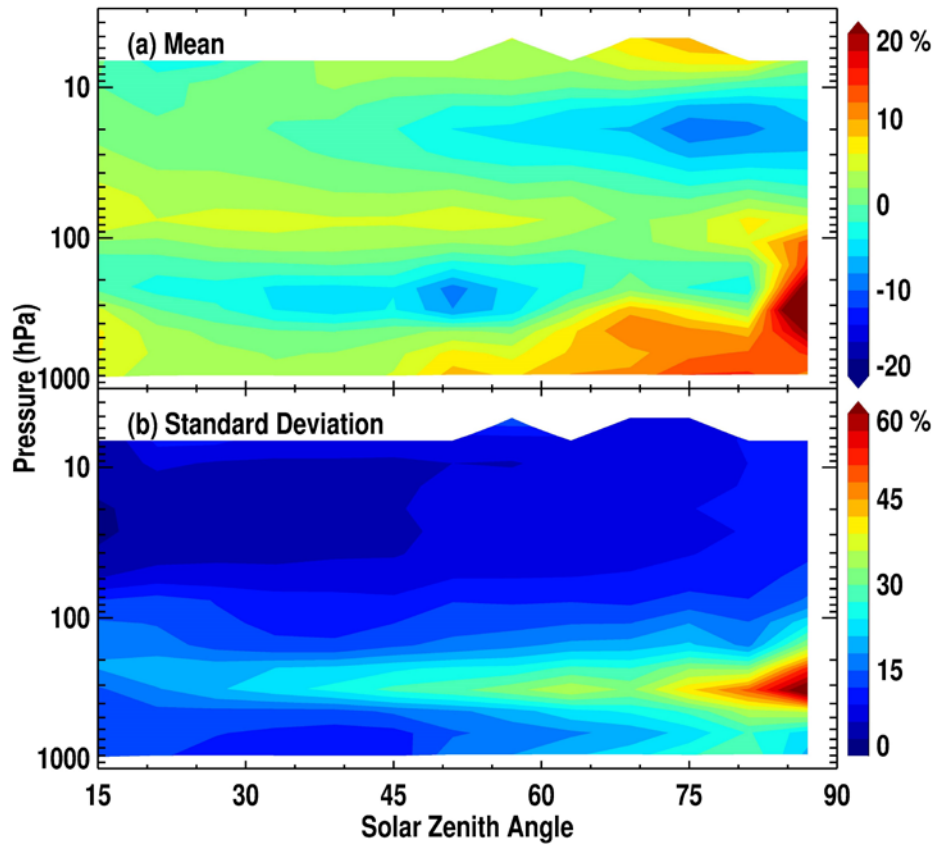
994



995

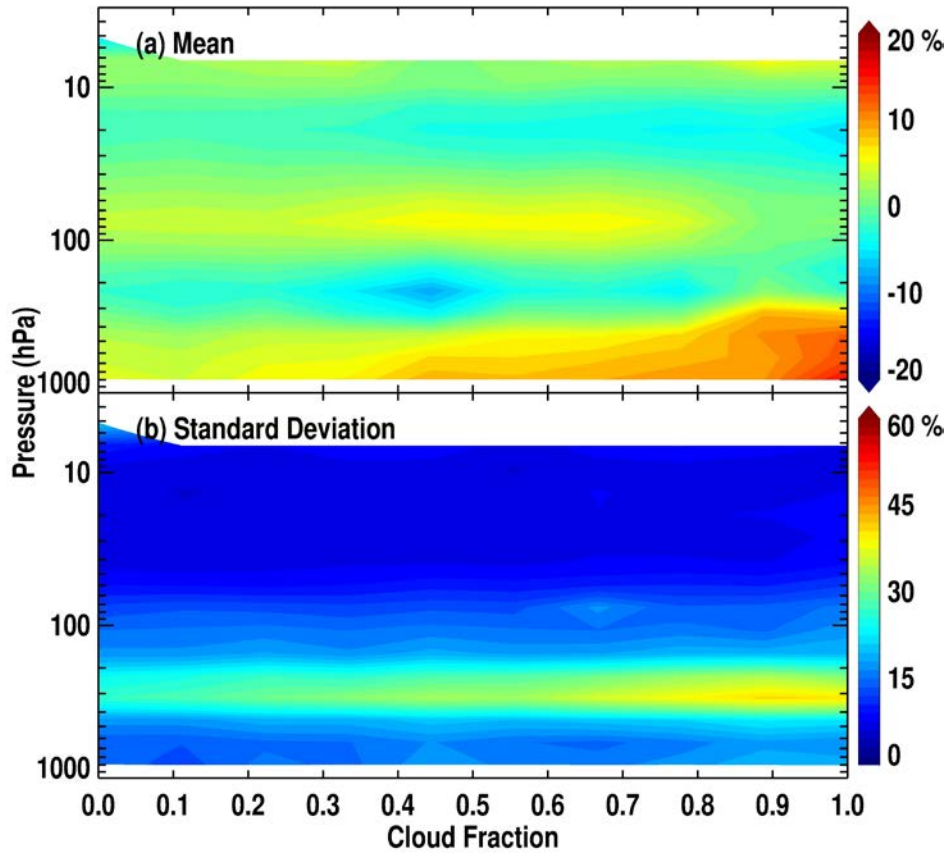
996 Figure 4 Same as Figure 3c but for each individual season at 30° N-60° N.

997



998
 999 **Figure 5** Mean relative biases in ozone (a) and standard deviations (b) of the differences between
 1000 OMI and ozonesonde convolved with OMI AKs as a function of Solar Zenith Angle using all
 1001 OMI/ozonesonde coincidences during 2004-2014.
 1002

1003



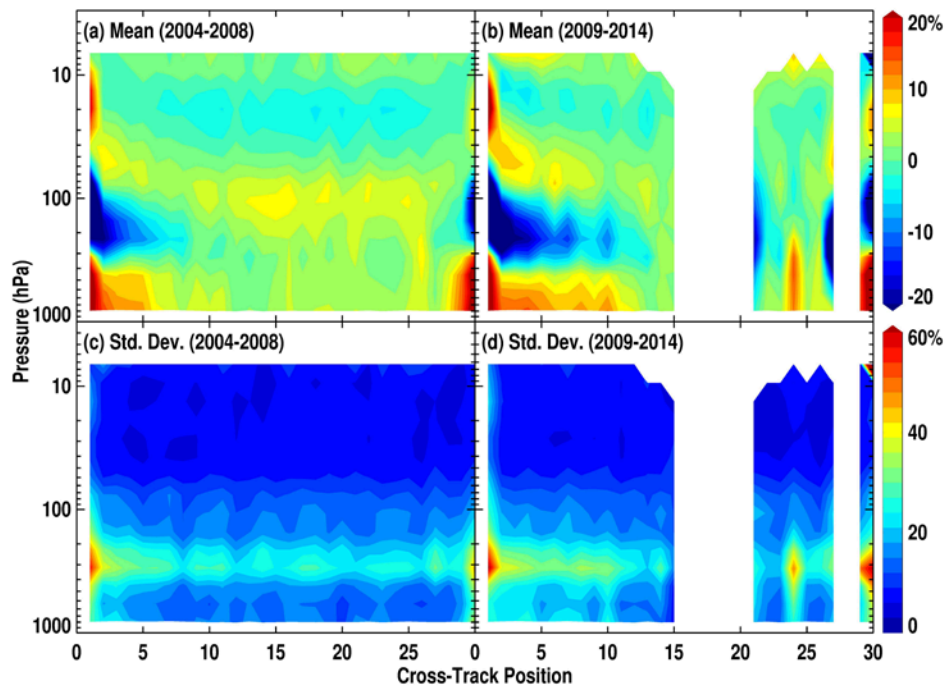
1004

1005 Figure 6 Same as Figure 5 but as a function of cloud fraction.

1006

1007

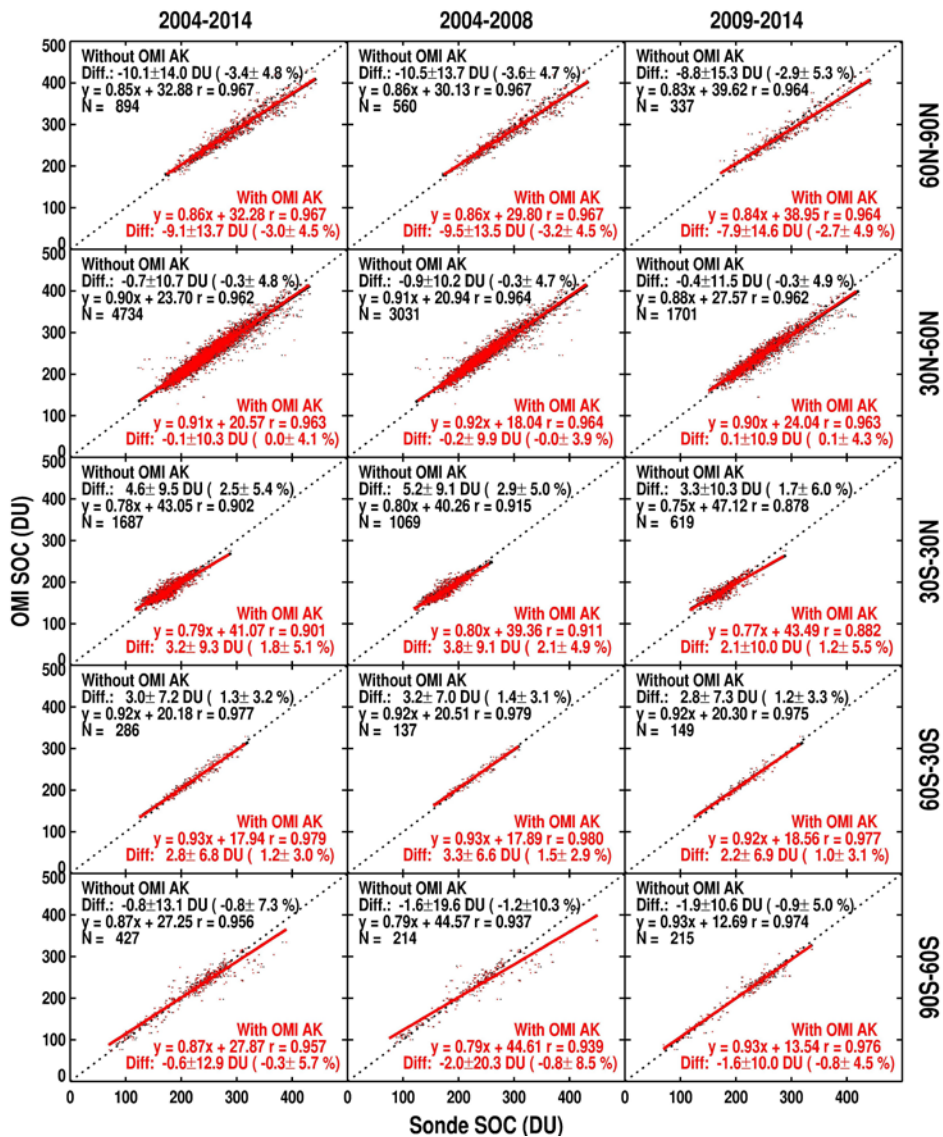
1008



1009

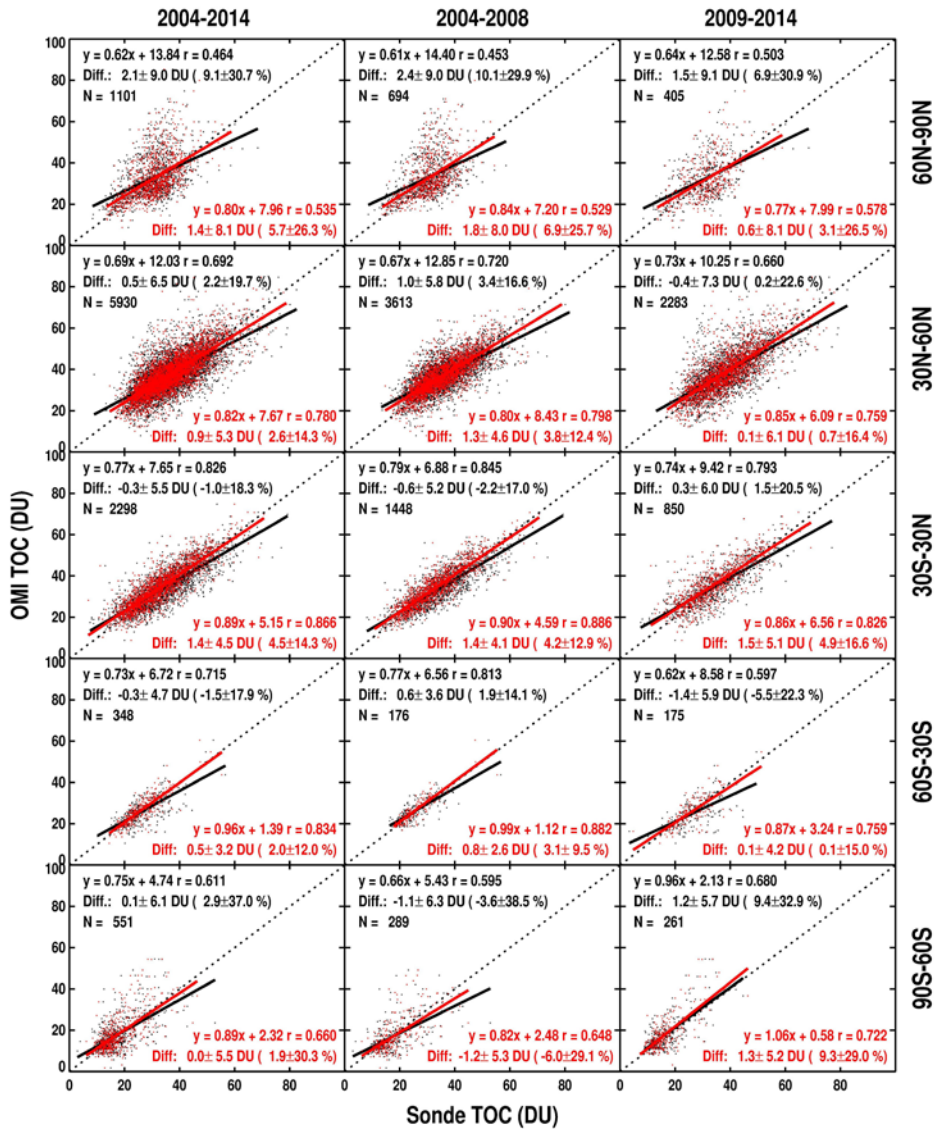
1010 Figure 7 Same as Figure 5 but as a function of cross-track position for (left) pre-RA (2004-2008)
1011 and (right) post-RA (2009-2014) periods, respectively.

1012



1013
 1014 Figure 8. Scatter plots of OMI Stratospheric Ozone Columns (SOCs) vs. ozonesonde SOC (DU)
 1015 without (black) and with (red) average kernels for five different latitude bands during 2004-2014
 1016 (left), the pre-row anomaly (RA) period (i.e., 2004-2008, middle) and the post-RA period (i.e., 2009-
 1017 2014, right), respectively. Comparison statistics including mean biases and standard deviations in

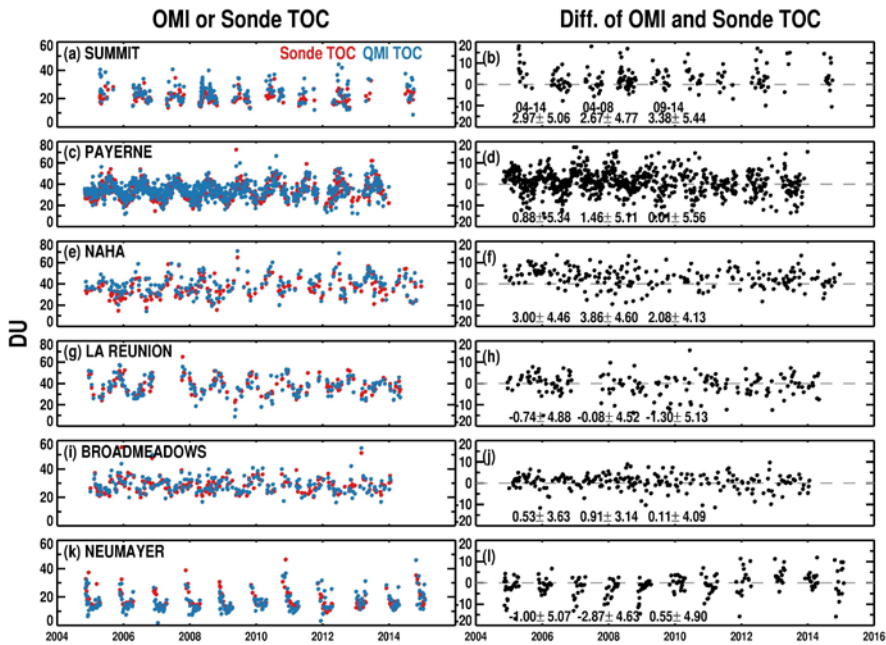
1018 both DU and %, the linear regression and correlation coefficients in DU, and the number of
1019 coincidences are shown in the legends.



1021

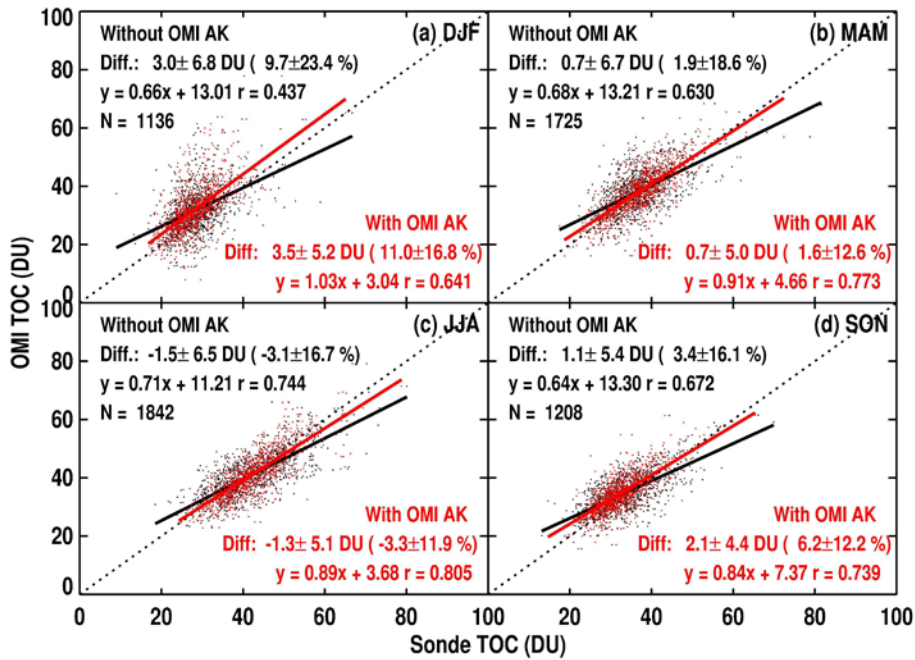
1022 Figure 9. Similar to Figure 8, but for comparison of Tropospheric Ozone Columns (TOCs).

1023



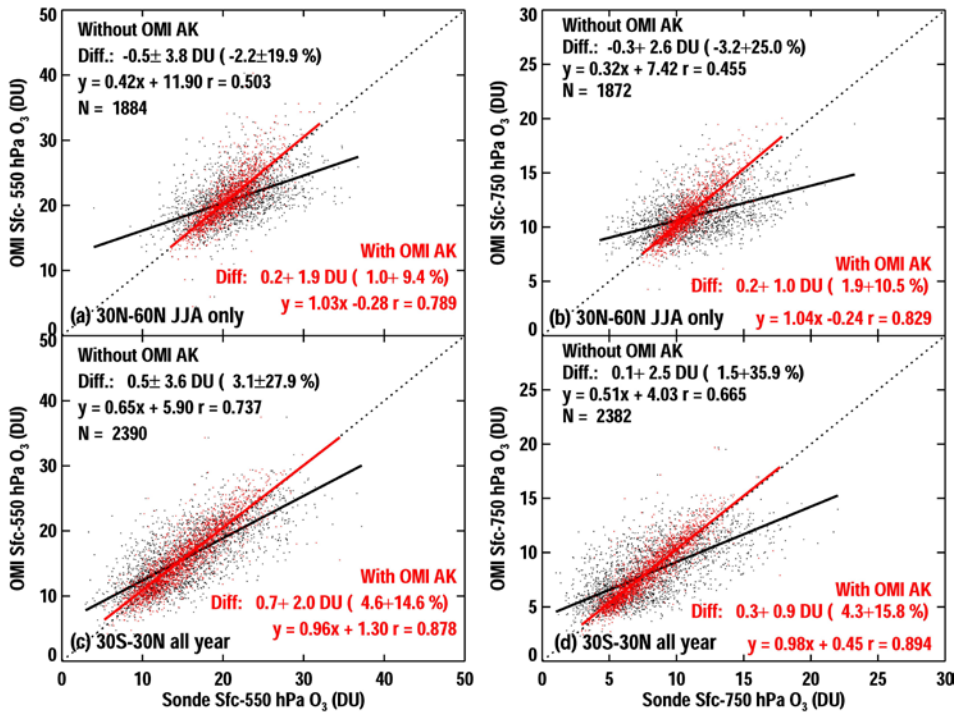
1024
 1025 **Figure 10.** (Left) Time series of OMI tropospheric ozone columns (TOCs) as green dots and
 1026 ozonesonde TOCs (with OMI AKs applied) in Summit (38.48° W, 72.57° N), Payene (6.57° E, 46.49°
 1027 N), Naha (127.69° E, 26.21° N), La Réunion (55.48° E, 21.06° S), Broadmeadows (144.95° E, 58.74°
 1028 S) and Neumayer (8.27° W, 70.68° S), and (Right) their corresponding differences, including the
 1029 mean biases and standard deviations in 2004-2014, pre-RA (2004-2008) and post-RA (2009-2014)
 1030 periods, respectively, in the legends.

1031



1032
 1033 Figure 11. Similar to Fig. 9 but for different seasons at northern middle latitude during the 2004-
 1034 2014 period.

1035



1037

1038

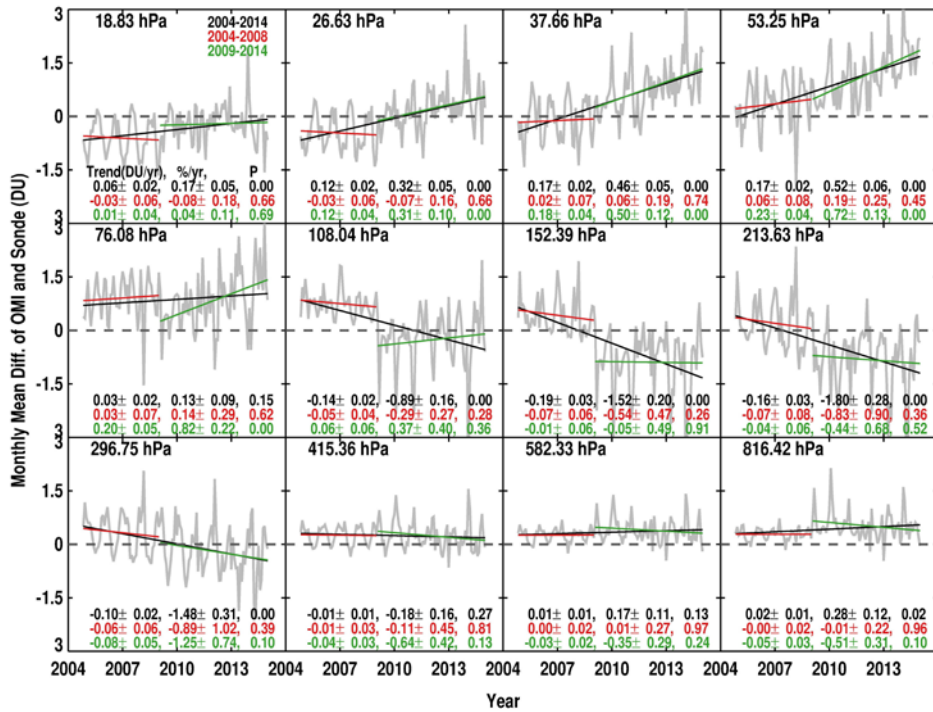
1039

1040

Figure 12. Similar to Fig. 9 but for comparison of lower tropospheric ozone columns during the 2004-2014 period. (a) Surface-550 hPa ozone column and (b) Surface-750 hPa ozone column in 30° N-60° N during the summer, (c) and (d) same as (a) and (b) but for the tropics.

1041

1042

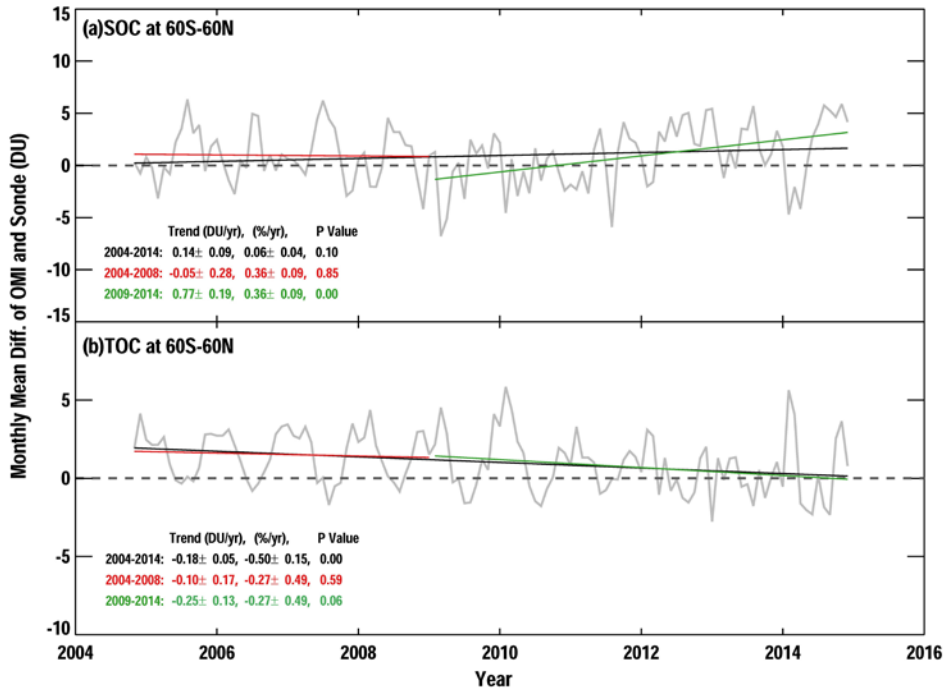


1043

1044 Figure 13. Monthly mean variation of OMI and ozonesonde mean biases in 60° N-60° S at each
 1045 OMI layer. OMI retrieval averaging kernels are applied to ozonesonde data. The black, red and
 1046 green lines represent the linear ozone bias trends in 2004-2014, pre-RA (2004-2008) and post-RA
 1047 (2009-2014), respectively. The average altitude of each layer is marked on the left corner of each
 1048 grid. The trends in DU/yr or % yr and P value for each time period are indicated in the legends.

1049

1050



1051

1052 Figure 14. Same as Figure 13 but for Stratospheric Ozone Columns (SOCs) and Tropospheric
1053 Ozone Columns (TOCs).